environmental microbiology

Environmental Microbiology (2020) **22**(9), 3863–3882 doi:10.1111/1462-2920.15160

High CO_2 concentration and iron availability determine the metabolic inventory in an *Emiliania huxleyi*-dominated phytoplankton community

Michaela A. Mausz,[1,2,7*] **María Segovia**,[3] **Aud Larsen**,[4,5] **Stella A. Berger**,[5,6] **Jorun K. Egge**[5] **and Georg Pohnert**[1*]

[1]*Department for Bioorganic Analytics, Friedrich Schiller University Jena, Lessingstr. 8, Jena, 07743, Germany.*
[2]*Leibniz Institute for Natural Product Research and Infection Biology, Hans Knöll Institute (HKI), Beutenbergstr. 11a, Jena, 07745, Germany.*
[3]*Department of Ecology, Faculty of Sciences, University of Málaga, Bulevar Louis Pasteur s/n, Málaga, 29071, Spain.*
[4]*NORCE Norwegian Research Centre AS, Nygårdsgaten 112, Bergen, 5038, Norway.*
[5]*Department of Biology, University of Bergen, Thormøhlensgaten 53A/B, Bergen, 5020, Norway.*
[6]*Department of Experimental Limnology, Leibniz-Institute of Freshwater Ecology and Inland Fisheries (IGB), Alte Fischerhütte 2, Stechlin, 16775, Germany.*
[7]*School of Life Sciences, The University of Warwick, Gibbet Hill Campus, Coventry, CV4 7AL, United Kingdom.*

Summary

Ocean acidification (OA), a consequence of anthropogenic carbon dioxide (CO_2) emissions, strongly impacts marine ecosystems. OA also influences iron (Fe) solubility, affecting biogeochemical and ecological processes. We investigated the interactive effects of CO_2 and Fe availability on the metabolome response of a natural phytoplankton community. Using mesocosms we exposed phytoplankton to ambient (390 µatm) or future CO_2 levels predicted for the year 2100 (900 µatm), combined with ambient (4.5 nM) or high (12 nM) dissolved iron (dFe). By integrating over the whole phytoplankton community, we assigned functional changes based on altered metabolite concentrations. Our study revealed the complexity of phytoplankton metabolism. Metabolic profiles showed three stages in response to treatments and phytoplankton dynamics. Metabolome changes were related to the plankton group contributing respective metabolites, explaining bloom decline and community succession. CO_2 and Fe affected metabolic profiles. Most saccharides, fatty acids, amino acids and many sterols significantly correlated with the high dFe treatment at ambient pCO_2. High CO_2 lowered the abundance of many metabolites irrespective of Fe. However, sugar alcohols accumulated, indicating potential stress. We demonstrate that not only altered species composition but also changes in the metabolic landscape affecting the plankton community may change as a consequence of future high-CO_2 oceans.

Received 20 January, 2020; accepted 8 July, 2020. *For correspondence. E-mail: michaela.mausz@gmail.com; Tel. +44 24 7652 2697. georg.pohnert@uni-jena.de; Fax number: +49 3641 9-401102, Tel. +49 3641 94870.

Introduction

Anthropogenic activities such as fossil fuel burning have caused an increase in atmospheric carbon dioxide (CO_2) since the industrial era (see Joos and Spahni, 2008; Tans and Keeling, 2020). The worst-case scenario, the Representative Concentration Pathway RCP 8.5 (IPCC, 2014), projects an increase in atmospheric CO_2 concentration above 1000 µatm by the end of this century. Unfortunately, the values predicted by the RCP 8.5 match concentrations measured in the atmosphere to date. Oceans are absorbing part of the carbon emissions resulting in a predicted pH reduction (termed ocean acidification, OA) of 0.4 units until the end of this century (Caldeira and Wicket, 2003). This will cause severe impacts on biodiversity, structure and function of coastal ecosystems (IPCC, 2019). Among the organisms most affected by OA are some phytoplankton groups. The increased partial pressure of gaseous CO_2 (pCO_2) influences the net specific growth rate, the elemental stoichiometry and the physiology of phytoplankton (Engel *et al*., 2005; Segovia *et al*., 2017). However, we still lack a coherent theoretical and empirical foundation for a complete understanding of how whole ecosystems will respond to global change (Ullah *et al*., 2018).

Mesocosm studies allow rigorous testing of global change impacts at the ecosystem level improving our

understanding of ecological responses to such changes because of their high degree of realism and predictive potential. Hence, mesocosm experiments fill the gap between small-scale laboratory experiments in which reality is somewhat distorted, and open ocean observations where identifying mechanistic relationships is difficult or impossible (Stewart *et al*., 2013; Riebesell and Gattuso, 2015).

Mesocosm experiments have indeed revealed that picoeukaryotes and some nano- and micro-eukaryotes can perform better at elevated CO_2 concentrations. However, coccolithophores may strongly be negatively impacted while cyanobacteria have shown both negative and positive responses to high CO_2 (Riebesell *et al*., 2017; Schulz *et al*., 2017; Segovia *et al*., 2017).

The coccolithophore *Emiliania huxleyi* is the most important calcifier in the world's oceans. Its abundance and calcifying activity results in a global importance of the species for biogeochemical cycles (Westbroek *et al*., 1989; Paasche, 2002). *Emiliania huxleyi* regulates the exchange of CO_2 across the ocean–atmosphere interface through the ratio of calcite precipitation to organic matter production (the rain ratio, Rost and Riebesell, 2004). Hence, it is crucial to understand potential feedbacks of increasing atmospheric CO_2, calcification, or a shift in the dominance of coccolithophores, to better forecast the effects of global change on our future oceans.

OA is one example stressor (or driver) but it is unlikely to occur in isolation; climate change will result in multiple stressors to organisms (Boyd *et al*., 2018). Indeed, OA also highly impacts biogeochemical processes such as trace metal availability to plankton communities (Hutchins *et al*., 2009; Millero *et al*., 2009; Hoffmann *et al*., 2012). Iron is an essential trace element for phytoplankton growth due to its key role in metabolic processes, i.e. another driver (Behrenfeld and Milligan, 2013). Its availability depends on changes in pH, dissolved Fe concentration in the water, concentration and strength of iron-binding organic ligands (OLs), and irradiance (Sunda and Huntsman, 1995; Maldonado and Price, 2001; Barbeau *et al*., 2003; Millero *et al*., 2009; Shi *et al*., 2010). Multiple stressors will affect ecosystems directly but also interact with each other in many ways. To date, most research has, however, considered a single stressor (Boyd *et al*., 2018).

In this context, we conducted a full factorial mesocosm experiment with combined manipulation of both pCO_2 and dFe levels (Fig. S1) to assess the single or interactive effects of pCO_2 and dFe on the plankton community (Segovia *et al*., 2017). The so altered community was investigated in the metabolomics-based study introduced here. The metabolome is the complete inventory of intracellular and extracellular small molecules (metabolites), synthetized mostly, but not exclusively, by enzymatic reactions (Goulitquer *et al*., 2012). In this experiment, the biomass of the coccolithophore *E. huxleyi* strongly increased under elevated dFe (induced by addition of desferrioxamine B, DFB) and ambient pCO_2 (LC) conditions, while increased pCO_2 levels (HC) diminished *E. huxleyi* and *Synechococcus* sp. biomass. However, increased dFe concentrations partly mitigated the clear negative effects of elevated pCO_2 on the coccolithophore's physiology (Segovia *et al*., 2017; Segovia *et al*., 2018).

Considering the interactive effects of CO_2 and iron, the question arises, if such an observed altered species composition leads to changes of the community metabolome, or if other players can take over the metabolic role of less favoured species. Metabolites present in a sample at a given time offer a valuable snapshot of what is happening at this time in the community and/or ecosystem, as a consequence of abiotic or biotic shifts. Thus, how the environment affects phytoplankton metabolic processes will structure their acclimation and adaptive success in a changing climate. For instance, pH regulates metals' chemistry in seawater (Millero *et al*., 2009; Hoffmann *et al*., 2012) and in turn, phytoplankton control the cycling of trace metals, their chemical speciation and distribution in the sea. They release organic compounds (metabolites that happen to be OLs such as mono- and polysaccharides among others) which again regulate metals' chemistry (Hassler and Schoemann, 2009; Hassler *et al*., 2011; Sunda, 2012). Consequently, metabolomic approaches allow the elucidation of the chemical compounds that mediate responses to changing environmental/ecological factors or interactions in a complex community (Kuhlisch and Pohnert, 2015). Such interactions might be dependent on the metabolome of the community, revealing new mechanisms for processes such as community functions, ultimately affecting the channelling of matter and energy between trophic levels.

A number of culture-based studies have targeted the intracellular or extracellular metabolome of *E. huxleyi* (Obata *et al*., 2013; Rosenwasser *et al*., 2014; Mausz and Pohnert, 2015; Wördenweber *et al*., 2018) observing specific exometabolic responses triggered by grazing (Poulson-Ellestad *et al*., 2016). (Info)chemicals produced by diatom prey might influence selective feeding of copepods with a preferential selection of cells in late stationary phase (Barofsky *et al*., 2010), and the fatty acid composition encountered by grazers determines carbon transfer between trophic levels (Müller-Navarra *et al*., 2000). However, these studies focused on cultures thereby disregarding more complex physiological responses in natural communities. Metabolomic approaches conducted under close to natural conditions are scarce, but a recent mesocosm study successfully combined metabarcoding with metabolic analysis to demonstrate the importance of phytoplankton-derived lipid and carbohydrate bioavailability for copepod prey selection (Ray *et al*., 2016).

The current work investigates global change multi-stressor effects on the metabolome of a plankton community in experimental mesocosms. The specific aim was to study how increased pCO_2 and changed Fe availability affect the metabolic profile of a phytoplankton community dominated by the coccolithophore *E. huxleyi*. We determined (i) the metabolome in relation to the community structure patterns and (ii) possible metabolic changes due to pCO_2 or dFe treatments. We hypothesized that the cell metabolism will respond to different individual or interactive global change stressors. The intensity of the resulting change will be related to the composition and abundance of metabolic compounds in each cell/functional group. Hence, individual metabolic changes will affect how the marine plankton community responds to climate-driven-stressors. This is of paramount relevance, due to the imminent implications for the structuring and functioning of plankton communities under high CO_2 oceans prognosed for the future, and also in order to gain deeper insights into the effects of climate change on marine plankton communities over the coming decades to centuries.

Results

Phytoplankton dynamics

Plankton community dynamics and their response to the applied treatments in the mesocosms are described in detail by Segovia *et al*. (2017). Here, we want to point out a two-phasic pattern of phytoplankton community succession (Fig. S2). Phase 1 (days 0–10) was characterized by a rapid breakdown of an initial *Skeletonema* sp.-dominated diatom bloom (Fig. S2g) accompanied by a transient maximum of picoeukaryotes (Fig. S2d), small and large nanoeukaryotes (Fig. S2e, f), and dinoflagellates (Fig. S2h), and, slightly delayed, bacteria (Fig. S2i) showed similar growth patterns and declined towards the end of phase 1 (Fig. S2). In phase 2 (days 11–22), *Emiliania huxleyi* (Fig. S2b) strongly increased in abundance especially in the LC+DFB treatment reaching a biomass of 1600 $\mu g\ C\ L^{-1}$. Neither HC+DFB (200 $\mu g\ C\ L^{-1}$) nor HC-DFB (78 $\mu g\ C\ L^{-1}$) exceeded the carbon biomass of the control (LC-DFB, 400 $\mu g\ C\ L^{-1}$) (Fig. S2b). Note that carbon biomass or intracellular metabolites refer to the particulate organic carbon (POC) quotas. While HC inhibited *E. huxleyi* growth by approximately 50% compared with LC, DFB addition increased dFe and favoured *E. huxleyi* growth (Segovia *et al*., 2017). In parallel, *Synechococcus* sp. (Figure S2c) responded similarly to both pCO_2 and Fe treatments and its abundance increased during the second phase. In contrast, small and large nanoeukaryotes (including, e.g. haptophytes except *E. huxleyi*) showed no treatment-specific responses regardless of the increase exhibited during phase 2 (Fig. S2e, f).

Metabolic analysis

Here we present the results of combining a metabolomic study with a natural community succession experiment driven by a multiple stressor scenario. To detect underlying patterns despite the high complexity of the obtained data, we applied a number of analysis strategies. We started analysing whether the conducted pCO_2 and Fe treatments affected the community metabolome when considering all acquired metabolome samples from the 22 days of the experiment. Due to the multivariate nature of the metabolome dataset, we needed a powerful multivariate data analysis tool as provided by a constrained ordination procedure. We decided to use a canonical analysis of principal coordinates (CAP) and addressed the *a priori* hypothesis whether different groups (treatment or stage of community succession) affected the community metabolome resulting in a discriminant analysis (CAP_{discr}). By interpreting variables (metabolites) as data vectors (objects with a magnitude and direction between a start and end point) in a multivariate space, the discriminant analysis aims to define discriminant functions that maximize the separation of objects deriving from different groups. Besides generating trace statistics, each variable gets assigned a correlation coefficient, a statistical measure for the strength of the relationship. These coefficients or 'loadings' indicate the weight and direction of each explanatory variable for the separation of objects along with each discriminant function (Anderson and Willis, 2003; Paliy and Shankar, 2016). Thus, the higher the absolute value (load) of a metabolite's correlation coefficient is, the stronger is the relationship. Furthermore, translating a metabolite's correlation coefficient into coordinates in a multivariate space provides the end point of a vector, whose direction represents its correlation to a group/treatment. Further details on this type of statistical analysis can be found in the experimental procedures.

Our analysis initially aimed to gain an overview of metabolic changes over the whole time-course including all obtained samples from mesocosms and the fjord water. After data processing and peak sum normalization, we on average obtained 398 ± 73 specific compounds that were consistently detected in all 269 analysed samples deriving from 11 mesocosms and the fjord (compare Table S1). Results from one of the mesocosms were excluded from all analyses because a forming crust of ferric material on the surface of a deployed measuring instrument interfered with intended perturbations (Segovia *et al*., 2017). In another 10 samples the number of detected compounds was below the selection criterion

(mean ± 2 × standard deviation) and therefore excluded from further analysis. After processing, we were able to analyse 333 compounds from 259 mesocosm and fjord samples that remained in the constrained statistical analysis.

Using this complete dataset of 259 samples, the statistical approach of CAP_{discr} separated fjord from mesocosm samples from day 4 onwards (first CAP axis: eigenvalue 0.80, correlation Δ^2 0.64) manifesting a significant shift in metabolites released by the mesocosm plankton community compared with their fjord origin. However, due to the high complexity of the complete dataset, we could not find any specific patterns related to pCO_2 or Fe treatments. Accordingly, treatments could not be separated (Fig. 1) by multivariate statistics as indicated by high misclassification (44.79%) of samples in the 'leave-one-out' test (Table 1).

Since with the first analytical approach we could not determine treatment effects or other patterns when considering all obtained data, we focused on the control treatment (LC-DFB) only and analysed whether metabolomic changes correlated with different phases along the plankton community development. Therefore, we split our data into subsets based on metabolic stages related to phytoplankton dynamics defined above (stage 1: days 4–10, stage 2: days 11–22), but included a stage 0 (days 0–3) during which no metabolic separation between mesocosms and the fjord water was observed. We initially tested this approach on the control as it best reflected a community not subjected to stressors.

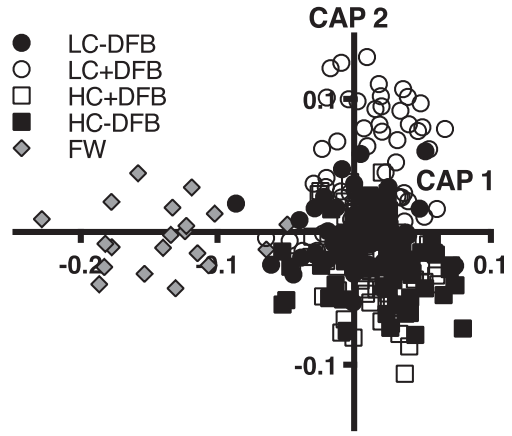

Fig 1. Multivariate separation of metabolic profiles deriving from mesocosms under different CO_2 and iron treatments from fjord water (FW) by canonical discriminant analysis of principal coordinates (CAP_{discr}) using a Bray–Curtis distance matrix. See Table 1 for statistical diagnostic values. Symbols represent 259 samples taken from mesocosms and fjord water (the latter: days 0–16 and 19–22) over a duration of 22 days. Phytoplankton communities within mesocosms were exposed to pCO_2 or iron treatments in triplicate ($n = 3$) except for LC-DFB where $n = 2$. Abbreviations: DFB, desferrioxamine B; HC, high pCO_2 (900 μatm); LC, ambient pCO_2 (390 μatm); pCO_2, partial pressure of gaseous carbon dioxide.

Further on, to better distinguish between phytoplankton dynamics and metabolic changes, we will use the term 'phase' for phytoplankton community succession steps (phase 1: days 0–10, phase 2: days 11–22), while metabolic responses shall be referred to as 'stages' (stage 0: days 0–3, stage 1: days 4–10, stage 2: days 11–22).

Metabolomic profiling of the control indicated metabolic shifts in accordance with community succession

We hypothesized that metabolic profiles followed a pattern related to community succession. To test this hypothesis, we applied the discriminant analysis-based CAP_{discr} to the control treatment (LC-DFB) using the three metabolic stages defined above as groups. We found that in control samples the three stages were well separated based on their metabolic profiles (eigenvalues 0.91, and 0.80, correlation Δ^2 0.83, and 0.64) (Table 1; Fig. 2). These results supported our hypothesis, thus we next determined which metabolites were responsible for the separation. A total of 152 out of 333 consistently detected compounds significantly correlated with either of the three stages. One hundred and five compounds (69.1%) could be identified or tentatively assigned to a biochemical class, the rest remained unknown (Figs 3 and 4).

Amines were among the metabolites (met.) that increased most pronouncedly in concentrations during stage 1: Ethanolamine, cadaverine and putrescine strongly correlated with stage 1 as did all detected amino acids (Figs 3 and 4, Fig. S3). Carboxylic acids either correlated with stage 0 or 1. For example, fumaric acid, and pyrrole-2-carboxylic acid (in two silylated forms) had vectors pointing towards stage 0 (Fig. 4a), whereas a benzoic acid derivative (met. 166), and malic acid strongly increased during stage 1 (up to 196-fold, and 27-fold more metabolite respectively) (Tables S2 and S3). The alcohol hexadecan-1-ol was associated with stage 1 as were most metabolites not assigned into a major metabolic class such as diethylenglycol or putative uridine (Figs 3 and 4A).

Saccharides and their derivatives exhibited a complex pattern with many monosaccharides significantly correlating with stage 0 or 1 while still showing low concentrations throughout the study (Figs 3 and 4B). Among them were, e.g. xylose, 2-O-glycerol-α-d-galactopyranoside and three pentafuranoses (met. 135, 136 and 143). Maltose, an unidentified disaccharide (met. 297), threonic acid and a hexonic acid (a hexose-derived sugar acid, met. 208) showed correlation to stage 0 and decreased in concentration toward stage 1 and 2. In contrast, pentonic acids (pentose-derived sugar acids, met. 169, and 173) exhibited the highest concentrations in stage 1 (Fig. 3). The galactoside digalactosylglycerol was

Table 1. Statistical diagnostic values of canonical discriminant analyses of principal coordinates (CAP_{discr}) including eigenvalue (λ) and squared correlation (Δ^2) for all CAP axes. Presented support values for pCO_2 and dFe treatments derived from CAP_{discr} of these factors only.

		Constrained canonical axes								Statistics	
		First axis		Second axis		Third axis		Fouth axis		Cross-validation	Permutation test
Treatments	Time[a]	λ	Δ^2	λ	Δ^2	λ	Δ^2	λ	Δ^2	Misclassification error (%)	Trace statistic
LC/HC, ±DFB, FW	All	0.80252	0.64404	0.67699	0.45832	0.57172	0.32687	0.37134	0.1379	44.79	0.0001
LC-DFB	All[b]	0.91204	0.83181	0.79974	0.63958					0.00	0.0001
LC/HC, ±DFB	Stage 0	0.70833	0.50174	0.5873	0.34191	0.44556	0.19852			62.16	0.3833
	Stage 1	0.69119	0.44774	0.25828	0.06671	0.165	0.02722			50.00	0.0015
	Stage 2[b]	0.93249	0.86954	0.84739	0.71807	0.46617	0.21732			23.2	0.0001
CO_2 (LC/HC)	Stage 2[b]	0.90999	0.82809							2.40	0.0001
dFe (±DFB)	Stage 2	0.63715	0.40596							28.80	0.0001
LC-DFB, LC+DFB, HC	Stage 2[b]	0.91476	0.83678	0.82989	0.68872					4.00	0.0001

Abbreviations: DFB, desferrioxamine B; +DFB, high dFe (12 nM); -DFB, ambient dFe (4.5 nM); dFe, dissolved iron; FW, fjord water; HC, high pCO_2 (900 µatm); LC, ambient pCO_2 (390 µatm); pCO_2, partial pressure of gas carbon dioxide.
[a]Stage 0: days 0–3, stage 1: days 4–10, stage 2: days 11–22.
[b]Metabolic profiles significantly separated treatments.

slightly elevated during stage 0 and the early days of stage 1 (Fig. 3). While an inositol isomer was higher abundant during stage 0, many sugar alcohols (e.g. mannitol, sorbitol, galactitol and viburnitol) increased during stage 2 (Fig. 3).

We could not see consistent correlation patterns in lipid classes. Many free fatty acids like myristic acid, 9-hexadecenoic acid and arachidonic acid showed higher concentrations during stage 0 and the early days of stage 1 but decreased in concentration over time toward stage 2, a pattern shared with the detected glyceride species 1-monohexadecanoylglycerol, and a C16:0-glycerol (met. 287). In contrast, other fatty acids correlated with stage 1 (Figs 3 and 4C). Most sterols increased in concentration over time and significantly correlated with stage 1 or 2 (Figs 3 and 4C). So, (22*E*)-26,27-dinoergosta-5,22-dien-3β-ol, (3β,5α)-cholestan-3-ol, fucosterol, beta-sitosterol, $C_{29}H_{52}O$ and $C_{29}H_{54}O$ correlated with stage 1, while e.g. epibrassicasterol, and stigmasterol separated stage 2. The oxoterpene *E*-phytol declined by 57%–86% during stage 2 in comparison to initial conditions (day 0) (Table S2). Additionally, unidentified metabolites were frequent during stage 0, but mostly correlated with stage 1 (Fig. 4D).

In summary, analysis of the control supported a three-stage metabolic pattern following phytoplankton community succession. We further successfully identified a number of metabolites that correlated with one of the three stages.

Single and interactive effects of pCO_2 and dFe

Although our analytical approach did not reveal a separation of treatments when the complete dataset including the

Fig 2. Multivariate separation of metabolic profiles in stage 0 (days 0–3), stage 1 (days 4–10) and stage 2 (days 11–22) in the control (LC-DFB) by CAP_{discr} using Bray–Curtis dissimilarities. Symbols represent 45 samples taken from duplicate mesocosms (one mesocosm on day 0) over a duration of 22 days. See Table 1 for statistical diagnostic values.

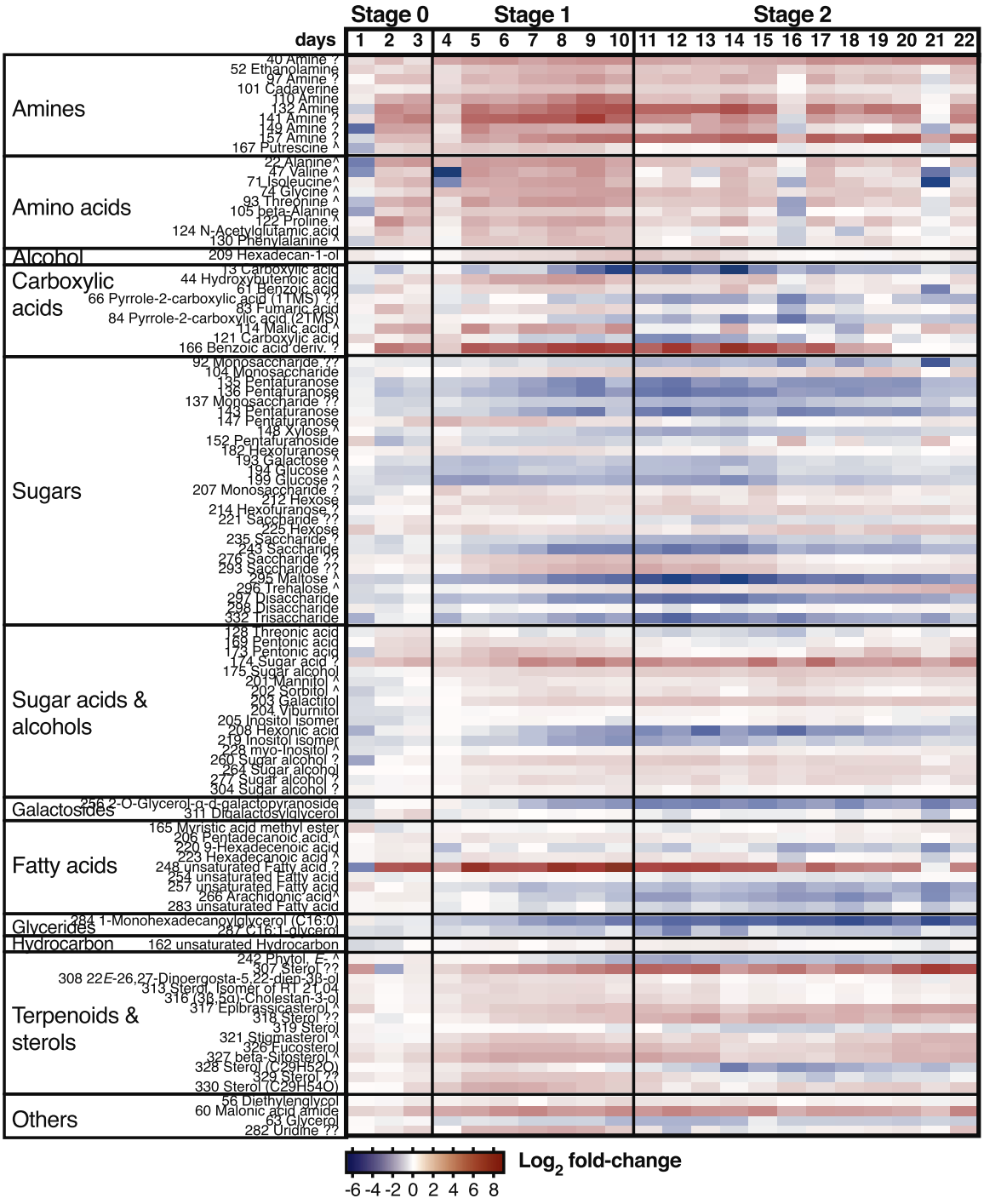

Fig 3. Heat map of $\log_2$ converted fold-changes in relation to initial conditions (day 0) for increased (black, print—red, online) or decreased (white, print—blue, online) metabolites significantly correlated with the control (LC-DFB) during stages 0, 1 and 2. Numbers represent metabolite identifiers (Tables S2 and S3). A caret indicates structure confirmation by standard or natural sample. Metabolites tagged with '?' possessed a reverse match of 700–800 and those with '??' one of 600–700. Data represent $\log_2$ converted fold-change of duplicate mesocosms ($n = 2$). Metabolomic data were normalized by peak sum. [Color figure can be viewed at wileyonlinelibrary.com]

fjord water was analysed, we assumed that treatment-related effects should become apparent over the course of the experiment. Hence, we next used CAP_{discr} to test whether we could find patterns related to pCO_2 and dFe treatments in the metabolic profiles during any of the three stages detected in the control.

The metabolic profiles of samples did not differ during stage 0 ($p = 0.3833$, permutation test) and half of them

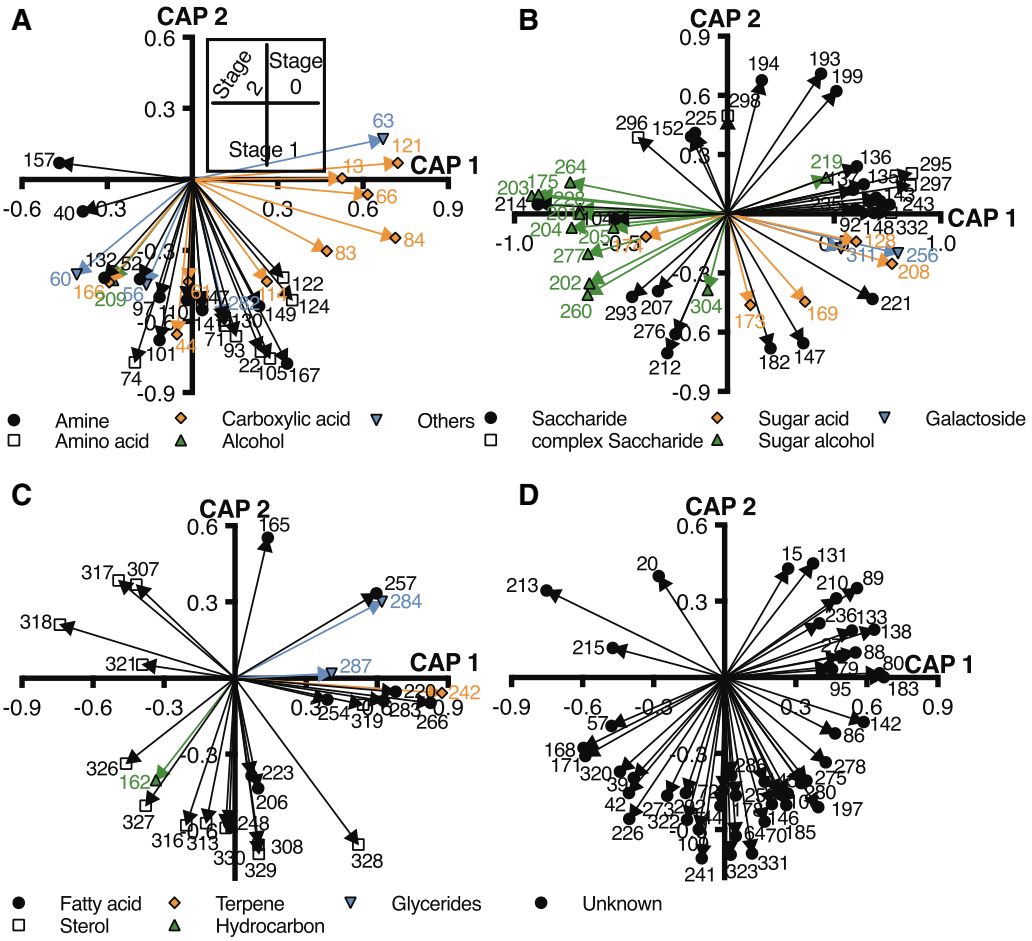

Fig 4. Vector plots of metabolites significantly correlated with the LC-DFB treatment (control) during stage 0 (days 0–3), stage 1 (days 4–10) or stage 2 (days 11–22) and belonging to (A) small compound classes or unassigned metabolites, (B) saccharides and other carbohydrates, (C) lipids, or (D) unknown metabolites. Numbers refer to metabolite identifiers (Tables S2 and S3). The inset positions metabolites in relation to metabolic stages. [Color figure can be viewed at wileyonlinelibrary.com]

were misclassified by cross-validation in stage 1 (Fig. 5A and B, Table 1) contradicting an early structuring effect of pCO_2 or dFe. However, during stage 2 the first CAP axis accounted for differences between LC and HC treatments, while the second axis separated between dFe treatments under LC (eigenvalue 0.93, and 0.85, correlation Δ^2 0.87, and 0.72), but failed to separate between HC+DFB and HC–DFB (Fig. 5C). Since the algorithm of CAP_{discr} produces (number of groups −1) axes, our dataset with four groups was reproduced in a three-dimensional space. But even the third axis failed to separate between dFe treatments under HC (eigenvalue 0.47, correlation Δ^2 0.22), and with 23.2% the misclassification error remained high during stage 2 (Table 1). Cross-validation performed by a 'leave-one-out' test could only correctly assign 69.7% of the samples to HC+DFB and correct placement decreased to 56.3% in HC-DFB, further confirming that there was no separation between HC treatments. To better understand how the treatments affected metabolic profiles, we analysed the main single effects of pCO_2 or dFe during stage 2. Metabolic profiles were significantly separated by pCO_2 as main effect during stage 2 (misclassification error 2.4%) (Table 1; Fig. 5D). In contrast, dFe alone did not significantly differentiate metabolic profiles (Fig. 5E), as the CAP axis failed to separate between +DFB and −DFB (eigenvalue 0.64, correlation Δ^2 0.41) resulting in 28.8% of samples being misclassified (Table 1). The inability to distinguish between metabolic profiles of HC+DFB and HC–DFB together with the findings that pCO_2 well separated metabolic profiles in accordance to treatments while dFe alone did not, lead us to the assumption that the four treatments did not evenly affect metabolic profiles. So as to best represent our metabolomic data and get the most information from data analysis, we decided to pool HC +DFB and HC–DFB samples resulting in three groups best demonstrating effects on metabolic profiles: LC-DFB, LC+DFB and HC (including both +DFB and -DFB).

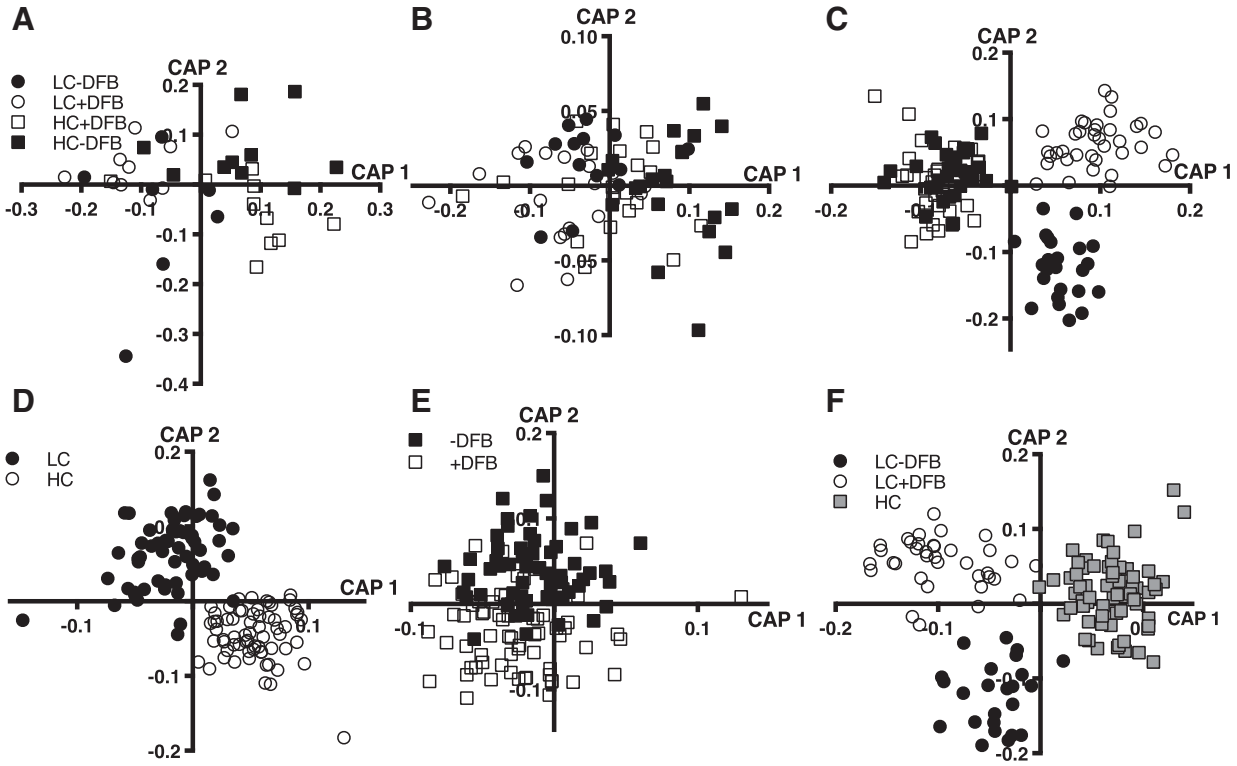

Fig 5. Multivariate separation of all treatments based on community metabolic profiles (A) in stage 0 (days 0–3), (B) stage 1 (days 4–10) and (C) stage 2 (days 11–22) of the mesocosm experiment by CAP_{discr} using Bray–Curtis dissimilarities. Effect of (D) pCO_2, and (E) dFe manipulation during stage 2, and (F) of a treatment combination (LC-DFB, LC+DFB, HC), which best represented metabolic profiles. See Table 1 for statistical diagnostic values. For better visualization, fjord samples were included in the analyses of pCO_2 and dFe (D, E) without plotting, as a CAP_{discr} on two groups results in a one-dimensional output. Abbreviations as in Fig. 1.

When these newly defined groups were tested by CAP_{discr}, the three groups formed well-separated clusters (Fig. 5F) with only 4.0% of the samples being misclassified by cross-validation (Table 1). This result confirmed that from a metabolomics perspective it was valid to combine HC+DFB and HC–DFB into a HC treatment, because metabolic profiles were nearly identical.

Overall, treatment effects just became apparent during metabolic stage 2 and we found that the four treatments only partially accounted for patterns of metabolic profiles during this stage. While pCO_2 affected the metabolism independent of the iron treatment, DFB addition influenced the community metabolome only under LC.

Metabolic profiling showed correlation of most metabolites with LC+DFB

After identifying that three treatments better represented our metabolic profiles during stage 2, we then examined which metabolites responded to which of the treatments. When treatments were grouped into LC-DFB, LC+DFB and HC in stage 2, 175 out of the 333 analysed detected compounds significantly correlated with the treatments. 113 (64.6%) could be identified or assigned to a metabolic class and 62 remained unknown (Figs 6 and 7). Below, we report metabolic responses based on pathways rather than treatments, because this best reflects the biochemistry of cells.

As noticed for the control, small metabolites such as amines or amino acids strongly increased in concentrations over time and most of them correlated with LC +DFB (Figs 6 and 7A, Fig. S4a). For example, an amine of the sum formula $C_{10}H_{17}NO$ (met. 33), and two putative amines (met. 40, and 141) correlated with LC+DFB, while hydroxylamine and ethanolamine showed highest concentrations under HC (Figs 6 and 7A). Amino acids (except glycine) and all detected TCA cycle substrates (succinic, fumaric, malic, and citric acid) increased more strongly under LC+DFB as did most of the remaining carboxylic acids (Fig. 6). The alcohols propane-1,3-diol, a long-chained alcohol (met. 271) and several metabolites not assigned into major classes (e.g. glycerol, lumichrome, trishydroxybenzene and putative adenosine) also significantly correlated with LC+DFB. In contrast,

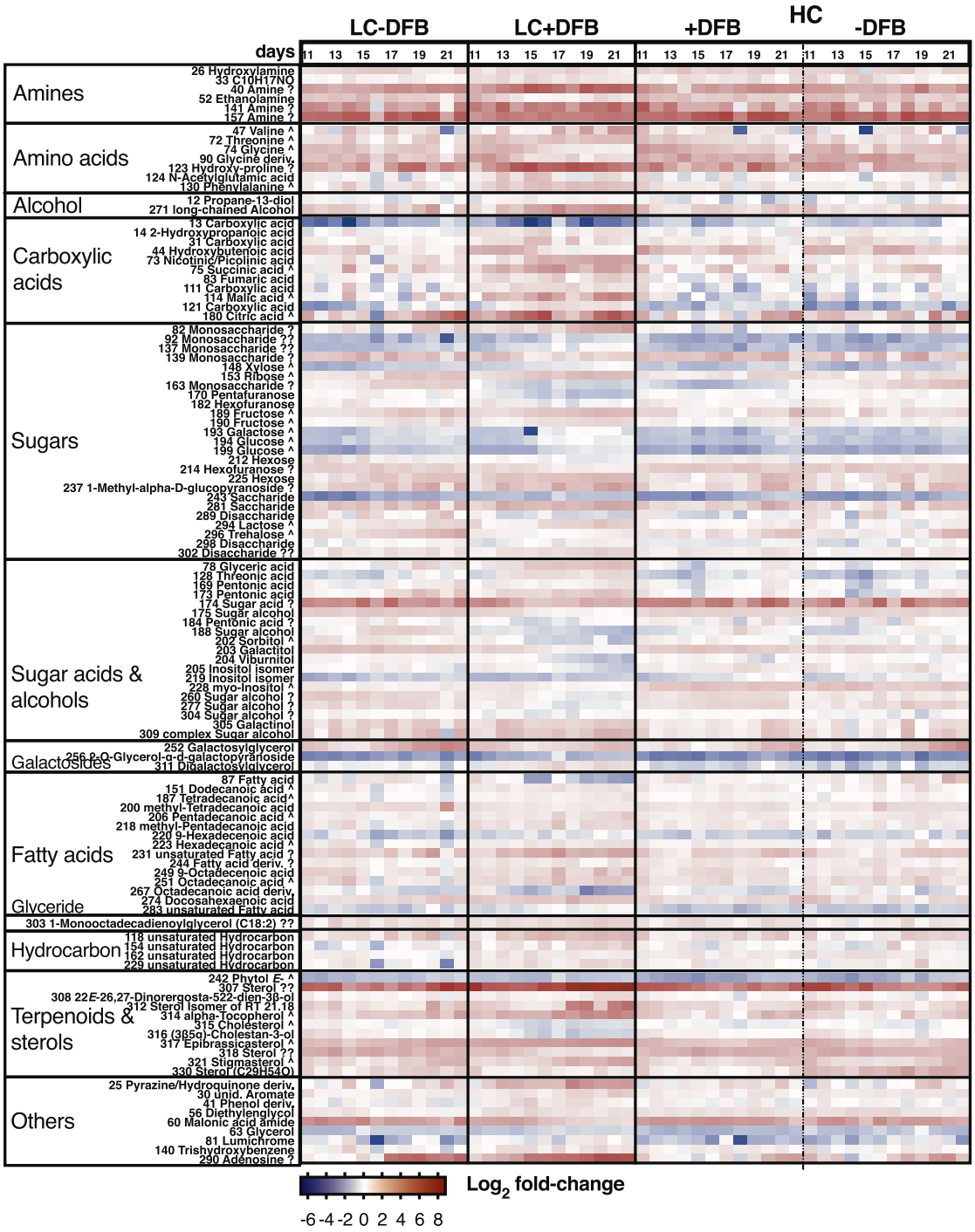

Fig 6. Heat map of $\log_2$ converted fold-changes in relation to initial conditions (day 0) for increased (black, print—red, online) or decreased (white, print—blue, online) metabolites significantly correlated with the treatments during stage 2. Numbers represent metabolite identifiers (Tables S2 and S3). A caret indicates structure confirmation by standard or a natural sample. Metabolites tagged with '?' possessed a reverse match of 700–800 and those with '??' one of 600–700. Data represent $\log_2$ converted fold-change of mean of triplicate mesocosms (n = 3) except for LC-DFB and a few data points with a replicate excluded from the analysis where n = 2 (see text). Metabolomic data were normalized by peak sum. Abbreviations as in Fig. 1. [Color figure can be viewed at wileyonlinelibrary.com]

diethylenglycol showed comparable abundance under LC +DFB and HC and a malonic acid amide correlated with both HC and LC-DFB (Figs 6 and 7A).

Among saccharides and their derivatives many were highly correlated with LC+DFB or were observed in comparable abundance in LC-DFB and HC as indicated by vectors

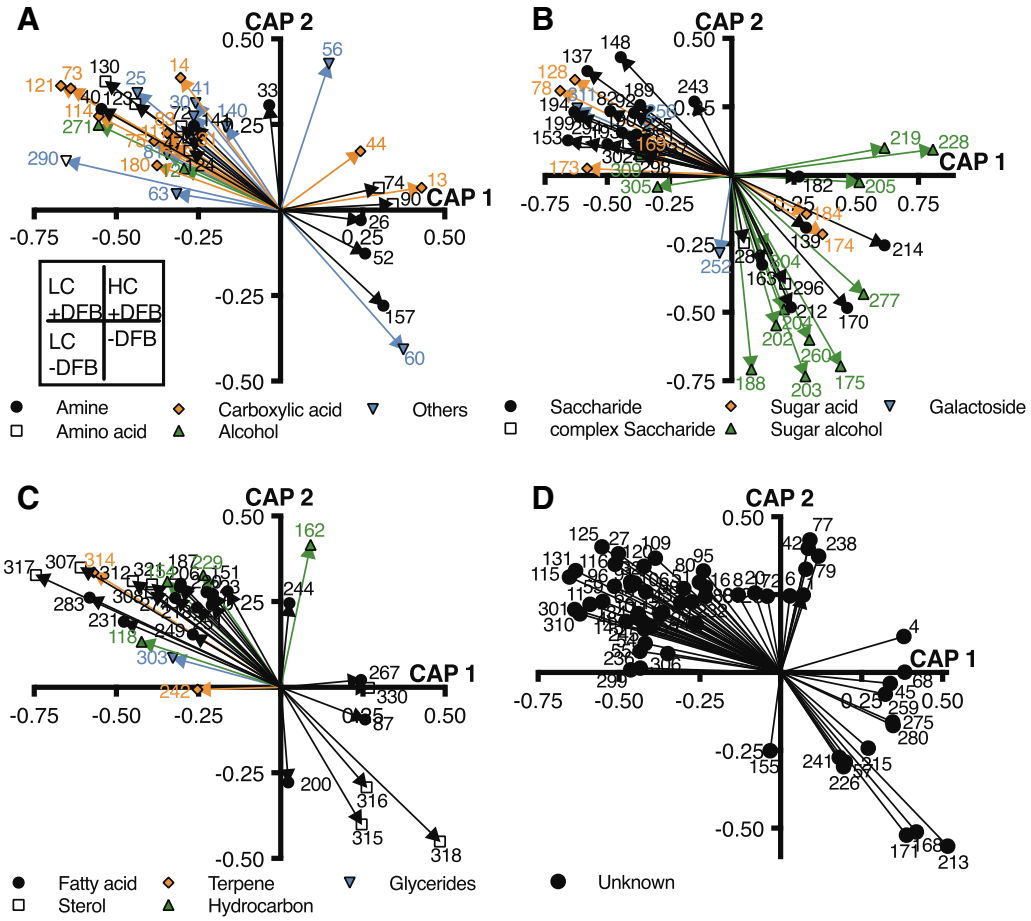

Fig 7. Vector plots of metabolites significantly correlated with all four treatments during stage 2 (days 11–22) and belonging to (A) small compound classes or unassigned metabolites, (B) saccharides and other carbohydrates, (C) lipids, or (D) unknown metabolites. Numbers refer to metabolite identifiers (Tables S2 and S3). The inset positions metabolites in relation to treatments. Abbreviations as in Fig. 1. [Color figure can be viewed at wileyonlinelibrary.com]

pointing between these treatments (Fig. 7B). Thus, xylose, ribose, fructose, galactose, glucose, 1-methyl-alpha-D-glucopyranoside and three out of five complex saccharides (lactose and two unidentified disaccharides, met. 298 and 302) were related to LC+DFB. In contrast, the galactoside galactosylglycerol increased strongest in the LC-DFB treatment (Fig. 6). Sugar acids either exhibited highest concentrations under LC+DFB (e.g. glyceric and threonic acid) or correlated with HC (Figs 5 and 7b). In contrast, all except two sugar alcohols (galactinol and another complex one, met. 309) significantly increased under HC or had vectors pointing between HC and LC-DFB (e.g. sorbitol, galactitol and viburnitol), thus, accounting for both treatments (Figs 6 and 7B).

Among lipids, correlations with LC+DFB dominated as observed for most free fatty acids. An exception provided an unidentified fatty acid (met. 87) and an octadecanoic acid derivative, which decreased in LC+DFB (Fig. 6). Methyltetradecanoic acid showed comparable abundances in HC and LC-DFB treatments (Fig. 6). Sterols mostly exhibited concentration increases during stage 2. (22*E*)-26,-27-dinorergosta-5,22-dien-3β-ol, epibrassicasterol and stigmasterol correlated with LC+DFB. However, cholesterol, (3β,5α)-cholestan-3-ol and a putative sterol (met. 318) similarly increased under HC and LC-DFB (Figs 6 and 7C). Furthermore, the terpenes *E*-phytol, which generally declined during stage 2, and alpha-tocopherol, as well as three unsaturated hydrocarbons (met. 118, 154 and 229) were affiliated to LC+DFB (Fig. 7C). Unidentified metabolites dominantly correlated with LC+DFB, but some also separated HC (Fig. 7D).

Discussion

Phytoplankton community responses to pCO_2 and iron treatments

In this mesocosm experiment we demonstrate that the phytoplankton community responded to changes in Fe availability and pCO_2 increase at the metabolic and at

the physiological level. This has major consequences for organisms belonging to the microbial loop and reaches out to higher trophic levels since they will be exposed to different interactions, communities, resources and regulators. Indeed, climate change can potentially weaken marine food webs through reduced energy flow to higher trophic levels, leading to food web simplification and altered producer–consumer dynamics (Ullah *et al*., 2018). For a better understanding of the processes relating to the treatments, we briefly summarize the mesocosm experiment results originating from Segovia *et al*. (2017) (Figs S1, S2, S5). High CO_2 levels significantly affected the chemical environment, due to the very dynamic speciation of particulate and dissolved trace metals occurring in Norwegian fjords (e.g. Fe; Öztürk *et al*., 2002). High CO_2, as well as the DFB addition elevated dFe concentration, and consequently increased Fe availability (see Segovia *et al*., 2017; Lorenzo *et al*., 2020 for further information). In the DFB treatments higher dFe concentrations were sustained, showing that DFB significantly increased the solubility of Fe, as previously reported (Chen *et al*., 2004) and demonstrated in this experiment by the calculation of Fe partitioning coefficients of the molar ratio between particulate and dissolved concentrations (see Fig. 4 in Lorenzo *et al*., 2020). A bloom of the coccolithophore *Emiliania huxleyi* was observed in the ambient CO_2 treatments, and was especially massive in the presence of DFB (LC+DFB). This result suggests that *E. huxleyi* is able to utilize DFB-bound Fe (Fe-DFB) (Segovia *et al*., 2017). *Emiliania huxleyi* produces a wide range of metabolites with a high affinity for Fe (Boye and van den Berg, 2000), and thus is able to acquire Fe from organic Fe complexes (Hartnett *et al*., 2012), including Fe-DFB (Shaked and Lis, 2012; Lis *et al*., 2015). While the biomass of *E. huxleyi* was negatively affected by increased CO_2 (Fig. S2b), increased dFe partially mitigated the negative effect of elevated CO_2, indicating that the coccolithophore was able to acclimate better to OA when Fe availability was high (Fig. S2b). High dFe also had a positive effect on the cyanobacterium *Synechococcus* sp. (Figure S2c) while the rest of the plankton food web did not respond to the treatments (Fig. S2d–i) (Segovia *et al*., 2017).

Phytoplankton showed a two-phasic succession pattern in response to increased pCO_2 and Fe availability as discussed by Segovia *et al*. (2017) with the most pronounced effect on the phytoplankton community observed in the LC treatment with elevated dFe (LC +DFB). A low Fe demand of the majority of phytoplankton groups except for *E. huxleyi* during phase 2 (Segovia *et al*., 2017) indicated that the dFe levels in the mesocosms were high enough to fulfil their Fe demands. In contrast, an array of symptoms indicative for Fe deficient algae (Behrenfeld and Milligan, 2013), including high Fe demand by the coccolithophore, reduced growth rates, lower Chl *a* and pigmentary content, low F_v/F_m and diminished photosynthesis, less DNA repair and poor ROS detoxification, were typical in the controls (LC-DFB) and strongly hinted Fe limitation for *E. huxleyi* in phase 2 (Segovia *et al*., 2017, 2018; Lorenzo *et al*., 2020).

Community metabolome reflects phytoplankton community changes within the control treatment

We assume that the control (LC-DFB) metabolic profiles reflected metabolic characteristics of a natural plankton community that switched from a diatom-dominated to a partly *E. huxleyi*-dominated bloom due to nutrient exhaustion after day 7. During stage 0 diatoms showed high abundances (Segovia *et al*., 2017), and also metabolic profiles denoted indication for a diatom-dominated community implied by the detection of 1-monohexadecanoylglycerol, a glyceride previously reported from a benthic diatom (Nappo *et al*., 2009). Additionally, indicators for *S. costatum* bloom decline occurred in the community meta-metabolome during stage 0. This persisted early in stage 1 while metabolome data also indicated a shift toward a mixed phytoplankton community, where *E. huxleyi* was already developing (Segovia *et al*., 2017). The contribution of bacterial groups to stage 1 of the community metabolome was neglectable irrespective of their abundances during plankton development (phase 1) due to low biomass of *Synechococcus* sp. in comparison to other phytoplankton groups, and the limitation of our filtration method in retaining heterotrophic bacteria (Lee *et al*., 1995; Mausz and Pohnert, 2015). The massive *E. huxleyi* biomass was the main contributor to metabolic profiles during stage 2 in the control.

Interpreting our findings constituted a challenge as the application of metabolomics is rarely used in analysing such complex communities as found in mesocosm experiments. With the exception of a recent study connecting copepod-prey selection to metabolic traits of the phytoplankton prey species (Ray *et al*., 2016), most mesocosm studies tend to limit complexity of investigated metabolic processes by targeted analyses, if these processes were at all considered. Commonly, effects of a specific compound class from a known producer, or targeted effects of toxicant or inhibitor addition at the community level, are quantified (Knauert *et al*., 2008; Liess and Beketov, 2011; Vidoudez *et al*., 2011; Paul *et al*., 2012). Hence, the lack of reference mesocosm-related metabolic profiles hitherto has necessitated a more indirect discussion with references to metabolomes of single species cultures.

Metabolic profiles of stage 0 were complex and subject to various patterns that partly transitioned into stage 1. Although several monosaccharides significantly correlated with stages 0 and 1, our data are in accordance

with decreasing overall carbon fixation rates during stage 0 due to the decline in diatoms (Lorenzo *et al*., 2018). Phosphorus starvation reportedly increased the sugar content in diploid *E. huxleyi* cultures (Wördenweber *et al*., 2018), and many saccharides exhibited slightly higher concentrations early in our experiment. This could be explained by photosynthesis still fuelling part of the energy needs of the cell, while downstream metabolism was increasingly halted due to nutrient conditions already limiting to a *S. costatum*-dominated diatom bloom during days 0–7. Our results are in agreement with higher glucose and polysaccharide levels reported in stationary *S. costatum* cells in culture (Vidoudez and Pohnert, 2012). Nutrient limitation downregulates the TCA cycle activity, leading to insufficient production of NADPH/ATP to maintain cell functioning and accumulation of TCA cycle metabolites (Wördenweber *et al*., 2018). This is consistent with highest concentrations of fumaric and malic acid in our metabolomic data during stages 0 and 1. Furthermore, pyrrole-2-carboxylic acid (correlated with stage 0) can derive from hydroxy-proline via an enzymatic or non-enzymatic reaction (Radhakrishnan and Meister, 1957) and its production is TCA cycle activity-dependent. The hypothetic scenario of a gradual metabolic shutdown described here, both conforms to metabolic data and the phytoplankton biomass development indicating the breakdown of an early diatom bloom.

Further support for a rapid decline in at least part of the phytoplankton community during the early days of the experiment can be found in lipid-associated metabolites detected during metabolic stages 0 or 1. Concentrations of an inositol isomer, glycerol and the glycoside digalactosylglycerol associated with stage 0 potentially derive from lipid breakdown. Linked to two fatty acids via glycerol, inositol forms the headgroup of the phospholipid phosphatidylinositol from which it can be enzymatically released (as phosphoinositol) by lipid degradation, e.g. during phosphorus starvation in plants (Nakamura, 2013) or in diatoms as observed in *Phaeodactylum tricornutum* (Brembu *et al*., 2017). In agreement to patterns observed in our experiment, digalactosylglycerol, the de-acylated form of galactolipids which occur in photosynthetic tissue of algae (van Hummel, 1975), accumulated during the stationary phase in *E. huxleyi* cell cultures (Mausz and Pohnert, 2015). Concomitantly, ethanolamine strongly increased during stage 1, hence, it might be similarly released from the lipid phosphatidylethanolamine indicating a progressing decay of cell membranes. The decaying diatom bloom is also reflected by high polyamine concentrations of putrescine and cadaverine during stage 1. Putrescine accumulated in declining diatom batch cultures (Vidoudez and Pohnert, 2012). Additionally, a study in the East China Sea documented increased polyamine concentrations after the dispersal of a *S. costatum* bloom when diatoms decomposed (Liu *et al*., 2016). These metabolic marker corroborate the breakdown of a diatom bloom accompanied by a community shift to pico- and nanoeukaryotes, dinoflagellates, and later to a high abundance of *E. huxleyi* in the control (Fig. S2) (Segovia *et al*., 2017).

We did not observe any sign of nitrogen limitation of phytoplankton growth during the experiment (Fig. S5). Limiting NO_3 concentration during phase 2 was compensated for by NH^+_4 via remineralization and nutrient release from the decaying diatom bloom in phase 1. Measured NH^+_4 levels of around 1.4 μM were well above the N demand of 0.78 μM N for individual phytoplankton groups (Segovia *et al*., 2017). Furthermore, we did not observe increases in C:Chl *a* ratios, which can be a proxy for N limitation (Jakobsen *et al*., 2015).

All detected amino acids correlated with metabolic stage 1 potentially provide a cellular pool of free amino acids that can serve as significant nitrogen buffer (Admiraal *et al*., 1986). Single species cultures confirm that amino acid production is high as long as nitrogen is not limited (Admiraal *et al*., 1986; Haberstroh and Ahmed, 1986). In iron-limited *P. tricornutum* cultures, increased glycolysis provided pyruvate-derived amino acids (of which isoleucine, valine and alanine were detected in our study) required for cellular proteome synthesis (Allen *et al*., 2008). As the community composition was diverse during phytoplankton phase 1 (Segovia *et al*., 2017), various species might have contributed to the amino acid pool in the metabolic stage 1 including *E. huxleyi* from which all detected amino acids except for *N*-acetylglutamic acid, have previously been reported (Obata *et al*., 2013; Mausz and Pohnert, 2015). Additionally, the complexity of sterols observed during stage 1 supports the assumption of a mixed community, reflecting the high variability of sterols in marine microalgae (Volkman, 2003). Fucosterol for instance dominates in brown algae (Patterson, 1971) and contributes up to 14% of total sterols in diatoms (Gladu *et al*., 1991). Sitosterol was found in high concentrations in the haptophyte *Diacronema (Monochrysis) lutheri* (Lin *et al*., 1982). Stigmasterol together with brassicasterol accounted for >75% of total sterols in haptophytes (Véron *et al*., 1996), although stigmasterol is not reported from the most abundant haptophyte, *E. huxleyi* (Maxwell *et al*., 1980; Mausz and Pohnert, 2015). Thus, we argue that the producers of the latter belonged to the small nanoeukaryote group that includes haptophytes and was present during stages 1 and 2.

Metabolic stage 2 manifested the high *E. huxleyi* abundance accompanied by first indications of bloom decline in the control. Mannitol, the main storage compound in *E. huxleyi* (Obata *et al*., 2013), accumulated during this period, as did epibrassicasterol, the dominant sterol in diploid *E. huxleyi* cells (Maxwell *et al*., 1980; Mausz and Pohnert, 2015). Induction of many sugar alcohols during

stage 2 indicated increasing stress as they can function as free radical scavengers (Raven and Beardall, 2003) and in culture accompanied algal decline (Mausz and Pohnert, 2015). Glucose slightly increased again with proceeding time after nutritional resources had been used up and it was no longer consumed in downstream glycolysis and energy production.

Treatments affect the community metabolome

Effects of treatments became apparent during metabolic stage 2. The metabolic community profiles diverged in response to pCO_2. In contrast, dFe only affected metabolic profiles in dependence of pCO_2, indicating an interacting effect on metabolism. Most metabolites correlated with LC+DFB, the treatment in which *E. huxleyi* massively bloomed due to increased dFe (Segovia *et al*., 2017). HC treatments did not result in *E. huxleyi* bloom development, and HC+DFB was not resolvable from HC-DFB by metabolic profiles. Nevertheless, increased dFe concentrations relieved cellular stress and enhanced photosynthetic activity in HC+DFB compared with HC-DFB (Lorenzo *et al*., 2018; Segovia *et al*., 2018). At the metabolic level, several metabolites (e.g. some of the sugar alcohols) positioned between LC-DFB (control) and HC (combining +DFB and -DFB treatments) in the CAP_{discr} analyses. This partial metabolic similarity of LC–DFB and HC could be linked to iron deficiency imposing a general stress, although most stress indicators correlated with HC treatments.

Correlation of the majority of amino acids (except glycine and its derivative, met. 90) to LC+DFB suggests high productivity situations. Valine directly derives from the glycolysis end product pyruvate, *N*-acetylglutamic acid is formed from glutamic acid and acetyl-CoA (Maas *et al*., 1953), and threonine, and hydroxy-proline descend from the TCA cycle receiving pyruvate via glycolysis. This demonstrates that high carbon fixation rates and glycolytic activity are necessary to sustain exponential growth. Indeed, increased Fe availability promoted the highest values of carbon fixation and particulate organic carbon accumulation at ambient pCO_2 during the bloom conditions (LC+DFB), as well as highest growth (Segovia *et al*., 2017; Lorenzo *et al*., 2018). Interestingly, all four detected TCA cycle intermediates correlated with LC +DFB as well. This is probably due to the requirement of iron as cofactor for aconitase, a key enzyme in the TCA cycle (Gray *et al*., 1993), and might indicate that high dFe concentrations in this treatment foster energy production via the TCA cycle (Segovia *et al*., 2017). In parallel, metabolites such as adenosine, and the pyridine derivatives nicotinic or picolinic acid increased, pointing to induced pyridine and purine biosynthesis for nucleotide production. Thus, we can legitimately suppose that nucleic acid and nucleotide biosynthesis are high in a fertile, growing population, since assessment of nucleic acid concentrations is used to quantify growth (e.g. Karl *et al*., 1981; Moriarty and Pollard, 1981). Supporting this, Segovia *et al*. (2018) found that DNA repair increased under LC+DFB as compared with the rest of the treatments.

Metabolome as well as physiological data revealed high photosynthetic activity and production of building blocks for cell growth and division. The photosynthetic electron transporter chain is highly iron-demanding making it vulnerable to iron stress (Raven *et al*., 1999), but under LC+DFB iron was plentiful favouring photosynthesis (Lorenzo *et al*., 2018; Segovia *et al*., 2018). This should result in the production of ATP, providing an additional explanation for the accumulation of adenosine, the head-group of ATP, visible in metabolic profiles. Photosynthetic energy generation could then fuel carbon fixation and subsequent creation of C3 sugars that could be converted into glucose. The latter then can be conveyed into glycolysis facilitating downstream metabolic reactions and promoting cell growth. Accordingly, we observed a slight increase in fructose, an early downstream product in glycolysis, as well as accumulation of sugar acids, particularly glyceric acid. If the enzymatic reducing capacity from photosynthesis in the presence of light is high, glycerate formation from CO_2 and accumulation is high (Tolbert, 1979) and this metabolite's relative intensity increases over further downstream products such as glycerol. This compound also accumulated in LC-treatments, while the effect gets reversed under iron limitation (Allen *et al*., 2008).

We confirmed a high complexity of sterols replicating the diversity of this compound class in phytoplankton (Volkman, 2003). Epibrassicasterol, the main sterol occurring in *E. huxleyi* (Maxwell *et al*., 1980), was highly abundant under LC+DFB probably due to the better performance of the coccolithophore. Effects of pCO_2 are unlikely as a previous laboratory-based study did not see huge changes in epibrassicasterol concentrations in *E. huxleyi* cultures under varying pCO_2 (Riebesell *et al*., 2000). Moreover, a consistent phytol content under changing pCO_2 (Riebesell *et al*., 2000) contrasts its correlation with LC+DFB reported here. Phytol constitutes the side-chain of chlorophyll *a* connected to its porphyrin backbone via an ester bond, but might also derive from chlorophyll *b*, *d*, or bacteriochlorophyll *a*. While chlorophyll *c* generally does not contain phytol, some haptophytes including *E. huxleyi* possess forms of unusual phytol-substituted chlorophyll *c* (e.g. Nelson and Wakeham, 1989; Zapata and Garrido, 1997). Thus, the correlation could also either reflect the general pattern of high photosynthetic activity or the high abundance of *E. huxleyi*. It might also relate to the correlation of the powerful radical-trapping antioxidant alpha-tocopherol (Palozza

and Krinsky, 1992) to LC+DFB. Its induction presumably lowered the stress experienced by algae as reported for plants (Munné-Bosch, 2005). Our metabolic data are also supported by the low oxidative stress detected in the LC +DFB treatment in this very experiment suggesting efficient free-radical scavenging mechanisms. Additionally, LC+DFB fostered the accumulation of key pigments such as fucoxanthins, chlorophyll *a* and *c*, promoting photosynthesis (Segovia *et al*., 2018).

HC treatments featured metabolites associated to stress

While LC+DFB generally induced favourable metabolic reactions, HC might have led to higher stress levels. Sugar alcohols, which mostly correlated with this treatment, can function as free radical scavengers (Raven and Beardall, 2003). The glycolytic derivative *myo*-inositol and its isomer were especially prominent, as an inositol dehydrogenase putatively allows haptophytes to use an inositol/inosase shuttle system for reducing equivalents between mitochondrion and cytosol (Gross and Meyer, 2003). As we see induced concentrations of glycine and its derivative, this reducing power exchange mechanism might have especial importance under the light of an intensified glycine and serine metabolism as it can mitigate the production of reactive oxygen species (Allen *et al*., 2008).

Ethanolamine, head-group of phosphatidylethanolamines, correlated with HC. Gordillo *et al*. (1998) reported that in nitrogen-limited *Dunaliella viridis* cultures, phosphatidylethanolamine concentrations were only affected by high pCO_2 (1%) but not ambient pCO_2. Their explanation of a relation to carbon availability does not fit the correlation patterns observed here. Almost all free fatty acids, the potential reaction partners to form phosphatidylethanolamine, were highest concentrated under LC. This contradicts a previous study reporting an increase in fatty acid cell content for all but highly unsaturated ones (C18:5 and C22:6) under increased pCO_2 conditions in *E. huxleyi* batch cultures (Riebesell *et al*., 2000). In our experiment, dFe might have overruled the potential pCO_2 effect as suggested in the physiology of *E. huxleyi* (Segovia *et al*., 2017, 2018). Thus, we speculate that the high abundance of fatty acids found in the blooming LC+DFB treatment could possibly mirror the generally high content of such storage lipids in algae (Griffiths and Harrison, 2009).

Concluding remarks

The present study supports the initial hypothesis that the individual or interactive stressors pCO_2 and dFe besides affecting species composition also impact the metabolic inventory of phytoplankton communities. Several metabolic changes could be explained by altered productivity of the system, and also by distinct changes that constitute stress markers and potential signalling molecules that are specifically induced during stress. We successfully traced certain metabolites to their putative producers within the phytoplankton community, but more importantly, we documented a bloom decline in the community metabolome.

Bioavailability is defined as the degree to which a certain compound can be accessed and utilized by an organism (reviewed in Shaked and Lis, 2012); on our case, Fe available for uptake, thus for growth. Sufficient bioavailable iron induced increased metabolic activity, and high amino and fatty acid biosynthesis under LC +DFB where *E. huxleyi* bloomed, as compared with LC-DFB. In contrast, HC lead to cellular stress responses. One could argue that the coccolithophore not only did benefit from more Fe, coping better with the stress driven by increased CO_2, but also it probably benefitted from reduced competition as other phytoplankton species were disadvantaged. Indeed, *E. huxleyi* gained a competitive advantage, but not because other phytoplankton species were disadvantaged due to decreased Fe availability, but because *E. huxleyi* presumably better met the metabolic requirements imposed by the encountered changed conditions as discussed by Segovia *et al*. (2017). The authors demonstrated that increased dFe during our experiment may have helped *E. huxleyi* cells to meet the extra metabolic demands imposed by the decrease in pH, allowing them to sustain growth due to the high Fe demand of this species vs. lower Fe demands of the other functional groups analysed. Within this scenario, some strains that are held back by iron limitation might become more abundant, gaining a competitive advantage through their low stringent requirements for nutrients and high growth under photoinhibitory conditions (traits not found in other functional groups) at increased Fe availability. The negative effects of OA on the development of ecologically and globally important species sensitive to increased CO_2 such as *E. huxleyi*, will be more relevant in high-Fe environments than in Fe-limited ones by possibly allowing a better stress management.

Thus, how the metabolic repertoire is affected, is key to unravel and predict changes to global change-driven-shifts at the community level. In a changing ocean, consumers in the plankton food web may encounter a modulated availability of resources, not only displayed by species but also by physiological changes. Hence, the altered phytoplankton meta-metabolome might affect the coupling between phytoplankton as primary and herbivores as secondary producers. Global change could then drive a marine food web collapse through altered trophic flows, a consequence of the global change scenario. Supposedly, what matters might not be the 'presence' of specific species, but rather, the metabolic composition

encountered by herbivores, phytoplankton, and heterotrophic bacterioplankton. Our study provides a predictive tool on specific resource availability in a rapidly changing marine plankton food web, which is of paramount relevance to understand what the future ocean may look like, attending to multiple stressors synergies and antagonistic effects.

Experimental procedures

Experimental design

The experimental work was carried out from 5 to 27 June 2012 in the Raunefjord (60.27°N, 5.22°E), off Bergen, Norway as described in detail by Segovia *et al*. (2017). We used a full factorial design with all combinations of ambient and elevated pCO_2 and dFe in three independent replicate mesocosms as detailed in the Supporting information. While two levels of CO_2 (LC, ambient pCO_2 at 390 μatm, and HC, high pCO_2 at 900 μatm) were achieved by addition of pure CO_2 gas, following recommendations by Marchetti and Maldonado (2016), changes in Fe availability were induced by amending half of the mesocosms with 70 nM (final concentration) of the siderophore desferrioxamine B (DFB) on day 7, when the community was already acclimated to high CO_2. Even though DFB is a strong Fe-binding OL often used to induce Fe limitation in phytoplankton (Wells, 1999), DFB additions may also increase the dissolved Fe pool in environments with high concentrations of colloidal and/or particulate Fe, such as fjords (Kuma and Matsunaga, 1995; Öztürk *et al*., 2002). In our experiment, the solubility of Fe in seawater was affected by either lowering the pH (Millero, 1998; Millero *et al*., 2009) and/or by the addition of DFB (Chen *et al*., 2004). The resulting multifactorial treatments were accordingly called LC-DFB (control), LC+DFB, HC+DFB and HC-DFB. Information on daily sampling of the mesocosms can be found in the Supporting information.

Plankton counts

Plankton analysis is described in detail by Segovia *et al*. (2017). Bacterioplankton and phytoplankton smaller than 20 μm were analysed by flow cytometry (Cytomics FC 500, Beckman Coulter, and FACSCalibur, Becton Dickinson respectively). Phytoplankton larger than 20 μm and microzooplankton were determined by using a FlowCAM (Fluid Imaging Technologies, USA).

Sampling of intracellular metabolites

Subsamples for monitoring intracellular metabolites were collected during daytime into 1 L plastic bottles (polypropylene, Nalgene®,VWR), since previous work in our group indicated an influence for sampling time mostly for differences in daytime vs. nighttime sampling (Vidoudez and Pohnert, 2012). Depending on *E. huxleyi* abundance, 3–6 L seawater were concentrated on GF/F glass fibre filters (mesh size ∼0.7 μm, Whatman) under medium vacuum (∼600 mbar), primarily retaining eukaryotic phytoplankton and larger bacteria such as cyanobacteria, since up to 87% of bacterioplankton cells can pass through GF/F filters (Lee *et al*., 1995). The performed 200 μm mesh pre-filtration in combination with the choice of GF/F glass fibre filters should have mostly prevented retaining non-target organisms. Filtrations were carried out under artificial light (PAR 150–200 μmol photons m^{-2} s^{-1}) and *in situ* temperature (∼10°C) to prevent temperature stress. Fjord water was sampled as a reference for metabolic changes. Cell filtration took 2–4 h per treatment. Wet filters were transferred into high-purity solvents (Chromasolv®, Chromasolv® Plus, Sigma-Aldrich; HiPerSolv, VWR) for metabolite extraction and stored at −80°C. Samples were processed within 1 month as described previously (Vidoudez and Pohnert, 2012; Mausz and Pohnert, 2015) with the following modifications: after extraction and drying for ∼5 h under reduced pressure (<30 mbar) samples were dried for another 1–2 h under further reduced pressure (<1 mbar) to ensure absolute dryness. For *N*-methyl-*N*-trifluoroacetamide (MSTFA)-derivatization the incubation temperature was increased from 40°C to 60°C.

GC–MS analysis and intracellular metabolite data processing

Gas chromatography mass spectrometry analysis conditions and conducted quality control measures are detailed in the Supporting information. Data processing was based on a published protocol (Vidoudez and Pohnert, 2012) and is further explained in the Supporting information. Data were normalized dividing each peak area by the sum of all peak areas within a biological replicate. This peak sum normalization delivers changes in the relative composition of the metabolome and avoids effects of different signal intensities caused by a variation of the overall metabolite content in the extracted cells as it could result from normalizing to, e.g. chlorophyll *a*. Due to the high complexity of the community, normalization by volume (litre) or biomass was not suitable for the obtained metabolomics data. For data presentation, $\log_2$ converted fold-change in relation to initial conditions (day 0) was calculated to distribute data around zero for better visualization.

Statistical analysis

Significant differences between pCO_2 and dFe treatments were evaluated by canonical analysis of principal coordinates (CAP). This multivariate approach performs

an initial principal coordinate analysis using any chosen distance or dissimilarity matrix followed by a discriminant analysis resulting in a canonical discriminant analysis of principal coordinates (CAP_{discr}). The multivariate data get reproduced onto a g-1 dimensional multivariate space with g equalling the number of groups (treatments) and orthogonal canonical axes that maximize differences among group locations (Anderson and Robinson, 2003; Anderson and Willis, 2003). We used CAP12 software (Anderson, 2004) with Bray–Curtis dissimilarity for the distance matrix and parameters according to Vidoudez and Pohnert (2012). CAP_{discr} is advantageous due to a very low sensitivity to hidden correlations, as needed for the application to metabolic samples containing amine derivatives. Moreover, it has the ability to analyse large multivariate datasets, and was previously successfully applied to microalgae metabolomes (Vidoudez and Pohnert, 2012; Paul *et al*., 2013; Rosenwasser *et al*., 2014; Mausz and Pohnert, 2015). We report statistical diagnostic values in the forms of eigenvalue (λ) and squared correlation (Δ^2). The eigenvalue indicates the efficiency of the axes in separating groups (the discriminating power), while Δ^2 specifies in how far axes are related to differences between groups. In addition, we obtained a *p*-value by permutation and performed cross-validation using the 'leave-one-out' approach, which obtains a misclassification error as estimate for the distinctness of groups in the multivariate space (Lachenbruch and Mickey, 1968). For CAP_{discr} all these parameters need to be considered when deciding about the statistical power of a test. In CAP_{discr} the explanatory variable (X) is composed of pairs of retention time and mass to charge ratio (*m*/*z*) with a responsive variable (Y) equalling the normalized peak area of each metabolite. Choosing a discriminant analysis approach additionally allowed us to determine the contribution of each metabolite (the explanatory variables) to the separation of groups based on their assigned weighted correlation coefficients (Paliy and Shankar, 2016). Correlations of metabolites with the CAP axes were considered significant, if they fall above a threshold correlation coefficient determined by a t-distribution with the corresponding degrees of freedom and a significance of $p = 0.01$. Visualization of correlation coefficients as vectors allowed their assignment to a specific treatment. The longer a vector is, the higher its correlation to a treatment distributed in the same direction with reference to the first two CAP axes.

Metabolite identification

Analysis of mass spectra to identify metabolites is described in detail in the Supporting information. Detailed information on measurement and peak annotation is provided in Table S4 based on recommendations by Fernie *et al*. (2011).

Acknowledgements

This work was supported by CTM/MAR 2010-17216 research grant (PHYTOSTRESS) from the Spanish Ministry for Science and Innovation (Spain) to M.S. G.P. acknowledges financial support by the CRC1127 ChemBioSys by the German Research Foundation. M.A.M. was supported by the EU FP7-INFRASTRUCTURE-2008-1 Project MESOAQUA (Network of leading MESOcosm facilities to advance the studies of future AQUAtic ecosystems from the Arctic to the Mediterranean) Grant No. 228224 (through the Transnational Access Program) and by a PhD studentship of the International Leibniz Research School for Microbial and Biomolecular Interactions (ILRS). S.A.B. was supported by the EU FP7-INFRASTRUCTURE-2008-1 Project MESOAQUA Grant No. 228224. A.L. was supported by the EU-ERC grant 250254 (MINOS) and the RCN project no. 225956/E10 (MicroPolar: Processes and Players in Arctic Marine Pelagic Food Webs – Biogeochemistry, Environment and Climate Change). We thank all participants of the PHYTOSTRESS project that helped setting up and sampling the mesocosms. We thank the staff at the Marine Biological Station (MBS) Espegrend, Norway, for logistic support. We also thank Prof. Ulrich S. Schubert for providing access to the flow cytometer to perform bacterial cell counts. We thank the two anonymous reviewers for very insightful comments and constructive criticisms.

References

Admiraal, W., Peletier, H., and Laane, R.W.P.M. (1986) Nitrogen metabolism of marine planktonic diatoms; extraction, assimilation and cellular pools of free amino acids in seven species with different cell size. *J Exp Mar Biol Ecol* **98**: 241–263.

Allen, A.E., LaRoche, J., Maheswari, U., Lommer, M., Schauer, N., Lopez, P.J., *et al*. (2008) Whole-cell response of the pennate diatom *Phaeodactylum tricornutum* to iron starvation. *Proc Natl Acad Sci U S A* **105**: 10438–10443.

Anderson, M.J. (2004) *CAP: A FORTRAN Computer Program for Canonical Analysis of Principal Coordinates*. New Zealand: Department of Statistics, University of Auckland.

Anderson, M.J., and Robinson, J. (2003) Generalized discriminant analysis based on distances. *Aust N Z J Stat* **45**: 301–318.

Anderson, M.J., and Willis, T.J. (2003) Canonical analysis of principal coordinates: a useful method of constrained ordination for ecology. *Ecology* **84**: 511–525.

Barbeau, K., Rue, E.L., Trick, C.G., Bruland, K.W., and Butler, A. (2003) Photochemical reactivity of siderophores produced by marine heterotrophic bacteria and cyanobacteria based on characteristic Fe(III) binding groups. *Limnol Oceanogr* **48**: 1069–1078.

Barofsky, A., Simonelli, P., Vidoudez, C., Troedsson, C., Nejstgaard, J.C., Jakobsen, H.H., and Pohnert, G. (2010)

Growth phase of the diatom *Skeletonema marinoi* influences the metabolic profile of the cells and the selective feeding of the copepod *Calanus* spp. *J Plankton Res* **32**: 263–272.

Behrenfeld, M.J., and Milligan, A.J. (2013) Photophysiological expressions of iron stress in phytoplankton. *Annu Rev Mar Sci* **5**: 217–246.

Boyd, P.W., Collins, S., Dupont, S., Fabricius, K., Gattuso, J.-P., Havenhand, J., *et al*. (2018) Experimental strategies to assess the biological ramifications of multiple drivers of global ocean change-a review. *Glob Chang Biol* **24**: 2239–2261.

Boye, M., and van den Berg, C.M.G. (2000) Iron availability and the release of iron-complexing ligands by *Emiliania huxleyi*. *Mar Chem* **70**: 277–287.

Brembu, T., Mühlroth, A., Alipanah, L., and Bones, A.M. (2017) The effects of phosphorus limitation on carbon metabolism in diatoms. *Philos Trans R Soc Lond B Biol Sci* **372**: 20160406.

Caldeira, K., and Wicket, M.E. (2003) Anthropogenic carbon and ocean pH. *Nature* **425**: 365.

Chen, M., Wang, W.-X., and Guo, L. (2004) Phase partitioning and solubility of iron in natural seawater controlled by dissolved organic matter. *Global Biogeochem Cy* **18**: GB4013.

Engel, A., Zondervan, I., Aerts, K., Beaufort, L., Benthien, A., Chou, L., *et al*. (2005) Testing the direct effect of CO_2 concentration on a bloom of the coccolithophore *Emiliania huxleyi* in mesocosm experiments. *Limnol Oceanogr* **50**: 493–507.

Fernie, A.R., Aharoni, A., Willmitzer, L., Stitt, M., Tohge, T., Kopka, J., *et al*. (2011) Recommendations for reporting metabolite data. *Plant Cell* **23**: 2477–2482.

Gladu, P.K., Patterson, G.W., Wikfors, G.H., Chitwood, D.J., and Lusby, W.R. (1991) Sterols of some diatoms. *Phytochemistry* **30**: 2301–2303.

Gordillo, F.J.L., Goutx, M., Figueroa, F.L., and Niell, F.X. (1998) Effects of light intensity, CO_2 and nitrogen supply on lipid class composition of *Dunaliella viridis*. *J Appl Phycol* **10**: 135–144.

Goulitquer, S., Potin, P., and Tonon, T. (2012) Mass spectrometry-based metabolomics to elucidate functions in marine organisms and ecosystems. *Mar Drugs* **10**: 849–880.

Gray, N.K., Quick, S., Goossen, B., Constable, A., Hirling, H., Kühn, L.C., and Hentze, M.W. (1993) Recombinant iron-regulatory factor functions as an iron-responsive-element-binding protein, a translational repressor and an aconitase. *Eur J Biochem* **218**: 657–667.

Griffiths, M.J., and Harrison, S.T.L. (2009) Lipid productivity as a key characteristic for choosing algal species for biodiesel production. *J Appl Phycol* **21**: 493–507.

Gross, W., and Meyer, A. (2003) Distribution of *myo*-inositol dehydrogenase in algae. *Eur J Phycol* **38**: 191–194.

Haberstroh, P.R., and Ahmed, S.I. (1986) Resolution by high pressure liquid chromatography of intracellular and extracellular free amino acids of a nitrogen deficient marine diatom, *Skeletonema costatum* (Grev.) Cleve, pulsed with nitrate or ammonium. *J Exp Mar Biol Ecol* **101**: 101–117.

Hartnett, A., Böttger, L.H., Matzanke, B.F., and Carrano, C.J. (2012) Iron transport and storage in the coccolithophore: *Emiliania huxleyi*. *Metallomics* **4**: 1160–1166.

Hassler, C.S., and Schoemann, V. (2009) Bioavailability of organically bound Fe to model phytoplankton of the Southern Ocean. *Biogeosciences* **6**: 2281–2296.

Hassler, C.S., Schoemann, V., Nichols, C.M., Butler, E.C., and Boyd, P.W. (2011) Saccharides enhance iron bioavailability to Southern Ocean phytoplankton. *Proc Natl Acad Sci U S A* **108**: 1076–1081.

Hoffmann, L.J., Breitbarth, E., Boyd, P.W., and Hunter, K.A. (2012) Influence of ocean warming and acidification on trace metal biogeochemistry. *Mar Ecol Prog Ser* **470**: 191–205.

Hutchins, D.A., Mulholland, M.R., and Fu, F. (2009) Nutrient cycles and marine microbes in a CO_2-enriched ocean. *Oceanography* **22**: 128–145.

IPCC. (2014) Climate change 2014: synthesis report. Contribution of working groups I, II and III to the fifth assessment report of the intergovernmental panel on climate change. In *Core Writing Team*, Pachauri, R.K., and Meyer, L.A. (eds). Geneva, Switherland: IPCC, p. 151.

IPCC. (2019) Summary for policymakers. In *IPCC Special Report on the Ocean and Cryosphere in a Changing Climate*, Pörtner, H.-O., Roberts, D.C., Masson-Delmotte, V., Zhai, P., Tignor, M., Poloczanska, E., *et al*. (eds).

Jakobsen, H.H., Blanda, E., Staehr, P.A., Højgård, J.K., Rayner, T.A., Pedersen, M.F., *et al*. (2015) Development of phytoplankton communities: implications of nutrient injections on phytoplankton composition, pH and ecosystem production. *J Exp Mar Bio Ecol* **473**: 81–89.

Joos, F., and Spahni, R. (2008) Rates of change in natural and anthropogenic radiative forcing over the past 20,000 years. *Proc Natl Acad Sci U S A* **105**: 1425–1430.

Karl, D.M., Winn, C.D., and Wong, D.C.L. (1981) RNA synthesis as a measure of microbial growth in aquatic environments. I. Evaluation, verification and optimization of methods. *Mar Biol* **64**: 1–12.

Knauert, S., Escher, B., Singer, H., Hollender, J., and Knauer, K. (2008) Mixture toxicity of three photosystem II inhibitors (antrazine, isoproturon, and diuron) toward photosynthesis of freshwater phytoplankton studied in outdoor mesocosms. *Environ Sci Technol* **42**: 6424–6430.

Kuhlisch, C., and Pohnert, G. (2015) Metabolomics in chemical ecology. *Nat Prod Rep* **32**: 937–955.

Kuma, K., and Matsunaga, K. (1995) Availability of colloidal ferric oxides to coastal marine phytoplankton. *Mar Biol* **122**: 1–11.

Lachenbruch, P.A., and Mickey, M.R. (1968) Estimation of error rates in discriminant analysis. *Dent Tech* **10**: 1–11.

Lee, S., Kang, Y.-C., and Fuhrman, J.A. (1995) Imperfect retention of natural bacterioplankton cells by glass fiber filters. *Mar Ecol Prog Ser* **119**: 285–290.

Liess, M., and Beketov, M. (2011) Traits and stress: keys to identify community effects of low levels of toxicants in test systems. *Ecotoxicology* **20**: 1328–1340.

Lin, D.S., Ilias, A.I.M., Connor, W.E., Caldwell, R.S., Cory, H. T., and Daves, G.D.J. (1982) Composition and biosynthesis of sterols in selected marine phytoplankton. *Lipids* **17**: 818–824.

Lis, H., Shaked, Y., Kranzler, C., Keren, N., and Morel, F.M. M. (2015) Iron bioavailability to phytoplankton: an empirical approach. *ISME J* **9**: 1003–1013.

Liu, Y., Zhao, W., Li, C., and Miao, H. (2016) Free polyamine content during algal bloom succession in the East China Sea in spring 2010. *Chin J Oceanol Limnol* **35**: 215–223.

Lorenzo, M.R., Iñiguez, C., Egge, J.K., Larsen, A., Berger, S.A., García-Gómez, C., and Segovia, M. (2018) Increased CO_2 and iron availability effects on carbon assimilation and calcification on the formation of *Emiliania huxleyi* blooms in a coastal phytoplankton community. *Environ Exp Bot* **148**: 47–58.

Lorenzo, M.R., Segovia, M., Cullen, J.T., and Maldonado, M. T. (2020) Particulate trace metal dynamics in response to increased CO_2 and iron availability in a coastal mesocosm experiment. *Biogeosciences* **17**: 1–14.

Maas, W.K., Novelli, G.D., and Lipmann, F. (1953) Acetylation of glutamic acid by extracts of *Escherichia coli*. *Proc Natl Acad Sci U S A* **39**: 1004–1008.

Maldonado, M.T., and Price, N.M. (2001) Reduction and transport of organically bound iron by *Thalassiosira oceanica* (Bacillariophyceae). *J Phycol* **37**: 298–310.

Marchetti, A., and Maldonado, M.T. (2016) Iron. In *The Physiology of Microalgae*, Borowitzka, M.A., Beardall, J., and Raven, J.A. (eds). Cham: Springer International Publishing, pp. 233–279.

Mausz, M.A., and Pohnert, G. (2015) Phenotypic diversity of diploid and haploid *Emiliania huxleyi* cells and of cells in different growth phases revealed by comparative metabolomics. *J Plant Physiol* **172**: 137–148.

Maxwell, J.R., Mackenzie, A.S., and Volkman, J.K. (1980) Configuration at C-24 in steranes and sterols. *Nature* **286**: 694–697.

Millero, F.J. (1998) Solubility of Fe(III) in seawater. *Earth Planet Sci Lett* **154**: 323–329.

Millero, F.J., Woosley, R., DiTrolio, B., and Waters, J. (2009) Effect of ocean acidification on the speciation of metals in seawater. *Oceanography* **22**: 72–85.

Moriarty, D.J.W., and Pollard, P.C. (1981) DNA synthesis as a measure of bacterial productivity in seagrass sediments. *Mar Ecol Prog Ser* **5**: 151–156.

Müller-Navarra, D.C., Brett, M.T., Liston, A.M., and Goldman, C.R. (2000) A highly unsaturated fatty acid predicts carbon transfer between primary producers and consumers. *Nature* **403**: 74–77.

Munné-Bosch, S. (2005) The role of α-tocopherol in plant stress tolerance. *J Plant Physiol* **162**: 743–748.

Nakamura, Y. (2013) Phosphate starvation and membrane lipid remodeling in seed plants. *Prog Lipid Res* **52**: 43–50.

Nappo, M., Berkov, S., Codina, C., Avila, C., Messina, P., Zupo, V., and Bastida, J. (2009) Metabolite profiling of the benthic diatom *Cocconeis scutellum* by GC-MS. *J Appl Phycol* **21**: 295–306.

Nelson, J.R., Wakeham S.G. (1989). A phytol-substituted chlorophyll *c* from *Emiliania huxleyi* (Prymnesiophyceae). *Journal of Phycology*, **25**: 761–766. http://dx.doi.org/10.1111/j.0022-3646.1989.00761.x.

Obata, T., Schoenefeld, S., Krahnert, I., Bergmann, S., Scheffel, A., and Fernie, A.R. (2013) Gas-chromatography mass-spectrometry (GC-MS) based metabolite profiling reveals mannitol as a major storage carbohydrate in the coccolithophorid alga *Emiliania huxleyi*. *Metabolites* **3**: 168–184.

Öztürk, M., Steinnes, E., and Sakshaug, E. (2002) Iron speciation in the Trondheim Fjord from the perspective of iron limitation for phytoplankton. *Estuar Coast Mar Sci* **55**: 197–212.

Paasche, E. (2002) A review of the coccolithophorid *Emiliania huxleyi* (Prymnesiophyceae) with particular reference to growth, coccolith formation, and calcification-photosynthesis interactions. *Phycologia* **40**: 503–529.

Paliy, O., and Shankar, V. (2016) Application of multivariate statistical techniques in microbial ecology. *Mol Ecol* **25**: 1032–1057.

Palozza, P., and Krinsky, N.I. (1992) β-Carotene and α-tocopherol are synergistic antioxidants. *Arch Biochem Biophys* **297**: 184–187.

Patterson, G.W. (1971) The distribution of sterols in algae. *Lipids* **6**: 120–127.

Paul, C., Mausz, M.A., and Pohnert, G. (2013) A co-culturing/metabolomics approach to investigate chemically mediated interactions of planktonic organisms reveals influence of bacteria on diatom metabolism. *Metabolomics* **9**: 349–359.

Paul, C., Reunamo, A., Lindehoff, E., Bergkvist, J., Mausz, M.A., Larsson, H., *et al*. (2012) Diatom derived polyunsaturated aldehydes do not structure the planktonic microbial community in a mesocosm study. *Mar Drugs* **10**: 775–792.

Poulson-Ellestad, K.L., Harvey, E.L., Johnson, M.D., and Mincer, T.J. (2016) Evidence for strain-specific exometabolomic responses of the coccolithophore *Emiliania huxleyi* to grazing by the dinoflagellate *Oxyrrhis marina*. *Front Mar Sci* **3**: 1.

Radhakrishnan, A.N., and Meister, A. (1957) Conversion of hydroxyproline to pyrrole-2-carboxylic acid. *J Biol Chem* **226**: 559–571.

Raven, J.A., and Beardall, J. (2003) Carbohydrate metabolism and respiration in algae. In *Photosynthesis in Algae*, Larkum, A.W.D., Douglas, S.E., and Raven, J.A. (eds). Dordrecht: Springer Netherlands, pp. 205–224.

Raven, J.A., Evans, M.C.W., and Korb, R.E. (1999) The role of trace metals in photosynthetic electron transport in O2-evolving organisms. *Photosynth Res* **60**: 111–150.

Ray, J.L., Althammer, J., Skaar, K.S., Simonelli, P., Larsen, A., Stoecker, D., *et al*. (2016) Metabarcoding and metabolome analyses of copepod grazing reveal feeding preference and linkage to metabolite classes in dynamic microbial plankton communities. *Mol Ecol* **25**: 5585–5602.

Riebesell, U., Bach, L.T., Bellerby, R.G.J., Monsalve, J.R.B., Boxhammer, T., Czerny, J., *et al*. (2017) Competitive fitness of a predominant pelagic calcifier impaired by ocean acidification. *Nat Geosci* **10**: 19–23.

Riebesell, U., and Gattuso, J.-P. (2015) Lessons learned from ocean acidification research. *Nat Clim Change* **5**: 12–14.

Riebesell, U., Revill, A.T., Holdsworth, D.G., and Volkman, J.K. (2000) The effects of varying CO_2 concentration on lipid composition and carbon isotope fractionation in *Emiliania huxleyi*. *Geochim Cosmochim Acta* **64**: 4179–4192.

Rosenwasser, S., Mausz, M.A., Schatz, D., Sheyn, U., Malitsky, S., Aharoni, A., *et al*. (2014) Rewiring host lipid metabolism by large viruses determines the fate of *Emiliania huxleyi*, a bloom-forming alga in the ocean. *Plant Cell* **26**: 2689–2707.

Rost, B., and Riebesell, U. (2004) Coccolithophores and the biological pump: responses to environmental changes. In *Coccolithophores: From Molecular Processes to Global*

Impact, Thierstein, H.R., and Young, J.R. (eds). Berlin, Heidelberg: Springer-Verlag, pp. 99–126.
Schulz, K.G., Bach, L.T., Bellerby, R.G.J., Bermúdez, R., Büdenbender, J., Boxhammer, T., *et al*. (2017) Phytoplankton blooms at increasing levels of atmospheric carbon dioxide: experimental evidence for negative effects on prymnesiophytes and positive on small picoeukaryotes. *Front Mar Sci* **4**: 64. https://doi.org/10.3389/fmars.2017.00064.
Segovia, M., Lorenzo, M.R., Iñiguez, C., and García-Gómez, C. (2018) Physiological stress response associated with elevated CO_2 and dissolved iron in a phytoplankton community dominated by the coccolithophore *Emiliania huxleyi*. *Mar Ecol Prog Ser* **586**: 73–89.
Segovia, M., Lorenzo, M.R., Maldonado, M.T., Larsen, A., Berger, S.A., Tsagaraki, T.M., *et al*. (2017) Iron availability modulates the effects of future CO_2 levels within the marine planktonic food web. *Mar Ecol Prog Ser* **565**: 17–33.
Shaked, Y., and Lis, H. (2012) Disassembling iron availability to phytoplankton. *Front Microbiol* **3**: 123.
Shi, D., Xu, Y., Hopkinson, B.M., and Morel, F.M.M. (2010) Effect of ocean acidification on iron availability to marine phytoplankton. *Science* **327**: 676–679.
Stewart, R.I.A., Dossena, M., Bohan, D.A., Jeppesen, E., Kordas, R.L., Ledger, M.E., *et al*. (2013) Chapter two - mesocosm experiments as a tool for ecological climate-change research. *Adv Ecol Res* **48**: 71–181.
Sunda, W. (2012) Feedback interactions between trace metal nutrients and phytoplankton in the ocean. *Front Microbiol* **3**: 204.
Sunda, W.G., and Huntsman, S.A. (1995) Iron uptake and growth limitation in oceanic and coastal phytoplankton. *Mar Chem* **50**: 189–206.
Tans, P., and Keeling, R.F. (2020). Trends in atmospheric carbon dioxide [WWW document]. URL https://www.esrl.noaa.gov/gmd/ccgg/trends/.
Tolbert, N.E. (1979) Glycolate metabolism by higher plants and algae. In *Photosynthesis II*, Gibbs, M., and Latzko, E. (eds). Berlin Heidelberg: Springer Verlag, pp. 338–352.
Ullah, H., Nagelkerken, I., Goldenberg, S.U., and Fordham, D.A. (2018) Climate change could drive marine food web collapse through altered trophic flows and cyanobacterial proliferation. *PLoS Biol* **16**: e2003446.
van Hummel, H.C. (1975) Chemistry and biosynthesis of plant galactolipids. In *Fortschritte der Chemie Organischer Naturstoffe/Progress in the Chemistry of Organic Natural Products*, Zechmeister, L., Herz, W., Grisebach, H., and Kirby, G.W. (eds). Wien: Springer Verlag, pp. 267–295.
Véron, B., Dauguet, J.-C., and Billard, C. (1996) Sterolic biomarkers in marine phytoplankton. I. Free and conjugated sterols of *Pavlova lutheri* (Haptophyta). *Eur J Phycol* **31**: 211–215.
Vidoudez, C., Nejstgaard, J.C., Jakobsen, H.H., and Pohnert, G. (2011) Dynamics of dissolved and particulate polyunsaturated aldehydes in mesocosms inoculated with different densities of the diatom *Skeletonema marinoi*. *Mar Drugs* **9**: 345–358.
Vidoudez, C., and Pohnert, G. (2012) Comparative metabolomics of the diatom *Skeletonema marinoi* in different growth phases. *Metabolomics* **8**: 654–669.
Volkman, J.K. (2003) Sterols in microorganisms. *Appl Microbiol Biotechnol* **60**: 495–506.
Wells, M.L. (1999) Manipulating iron availability in nearshore waters. *Linmol Oceanogr* **44**: 1002–1008.
Westbroek, P., Young, J.R., and Linschooten, K. (1989) Coccolith production (biomineralization) in the marine alga *Emiliania huxleyi*. *J Protozool* **36**: 368–373.
Wördenweber, R., Rokitta, S.D., Heidenreich, E., Corona, K., Kirschhöfer, F., Fahl, K., *et al*. (2018) Phosphorus and nitrogen starvation reveal life-cycle specific responses in the metabolome of *Emiliania huxleyi* (Haptophyta). *Limnol Oceanogr* **63**: 203–226.
Zapata, M., Garrido J.L. (1997). Occurrence of phytylated chlorophyll *c* in *Isochrysis galbana* and *Isochrysis* sp. (clone T-ISO) (Prymnesiophyceae). *Journal of Phycology*, **33**: 209–214. http://dx.doi.org/10.1111/j.0022-3646.1997.00209.x.

Supporting Information

Additional Supporting Information may be found in the online version of this article at the publisher's web-site:

Table S1 Average number of detected metabolites.

Table S4. Summary of parameters used for peak annotation based on recommendations by Fernie *et al*. (20112011).

Fig. S1. Temporal development of (a) partial pressure of gaseous carbon dioxide (pCO_2), and (b) dissolved iron (dFe) due to desferrioxamine B (DFB) addition and pCO_2. Figure reproduced with permission from Segovia *et al*. (2017).

Fig. S2. Temporal development of chlorophyll *a* ($\mu g\ L^{-1}$), phytoplankton, and heterotrophic bacterioplankton biomass ($\mu g\ C\ L^{-1}$) in the mesocosms exposed to different CO_2 and dissolved iron (dFe) treatments. (a) Chlorophyll *a*, (b) *Emiliania huxleyi* (5–10 μm), (c) *Synechococcus* sp. (0.6–2 μm), (d) picoeukaryotes (0.1–2 μm), (e) small nanoeukaryotes (prasinophytes, small haptophytes, 2–7 μm), (f) large nanoeukaryotes (small single-celled diatoms and flagellated forms, 6–20 μm), (g) diatoms (chain-forming *Skeletonema* sp. 20- > 500 μm), (h) dinoflagellates (20–200 μm), (i) heterotrophic bacterioplankton (0.2–0.7 μm). Symbols indicate mean measurement of three independent mesocosms (n = 3) except for LC-DFB where n = 2. Error bars denote standard deviations. Abbreviations: DFB, desferrioxamine B; HC, high pCO_2 (900 μatm); LC, ambient pCO_2 (390 μatm); pCO_2, partial pressure of gaseous carbon dioxide. Figure reproduced with permission from Segovia *et al*. (2017).

Fig. S3. Vector plots (one vector exemplified, symbols showing vector heads) of metabolites significantly correlated with the LC-DFB treatment (control) during stage 0 (days 0–3), stage 1 (days 4–10), or stage 2 (days 11–22) and belonging to (a) small compound classes or unassigned metabolites, (b) saccharides and other carbohydrates, (c) lipids, or (d) unknown metabolites. Numbers refer to metabolite identifiers (Supporting information Table S2, S3). The insert positions metabolites in relation to metabolic stages. This figure corresponds to Fig. 4 except that only vector heads are presented for increased readability of metabolite identifiers.

Fig. S4. Vector plots (one vector exemplified, symbols showing vector heads) of metabolites significantly correlated with all four treatments during stage 2 (days 11–22) and belonging to (a) small compound classes or unassigned metabolites, (b) saccharides and other carbohydrates, (c) lipids, or (d) unknown metabolites. Numbers refer to metabolite identifiers (Supporting information Table S2, S3). The insert positions metabolites in relation to treatments. This figure corresponds to Fig. 7 except that only vector heads are presented for increased readability of metabolite identifiers.

Fig. S5. Temporal development of major nutrient concentrations within the mesocosms in the different treatments (LC: ambient CO_2 (390 μatm); HC: increased CO_2 (900 μatm); -DFB: no DFB addition; +DFB: with a 70 nM DFB addition): (a) nitrate, (b) ammonium, (c) silicic acid, (d) soluble reactive phosphate (SRP). Figure reproduced with permission from Segovia *et al*. (2017).

Table S2 Fold-changes in relation to pre-experimental conditions (day 0) of increased (red) and decreased (blue) detected metabolites for pCO_2 and dFe treatments in the mesocosms. A caret indicates a structure confirmed by standard or a natural sample. Metabolites tagged with '?' possessed a reverse match of 700–800 and those with '??' one of 600–700. Data represent fold-change of mean of triplicate mesocosms (n = 3) except for LC-DFB (n = 2) and a few data points, where we had to exclude a replicate as outlier, where n = 2 (see text). Metabolomic data have been normalized by peak sum. The column 'Treatment' refers to the treatment(s) a metabolite significantly correlated with. Abbreviations: A, amine; AA, amino acid; Alc, alcohol; CA, carboxylic acid; CS, complex saccharide; D, day; DFB, desferrioxamine B; dFe, dissolved iron; FA, fatty acid; G, glyceride; Ga, galactoside; HC, high pCO_2 (900 μatm); HY, hydrocarbon; LC, ambient pCO_2 (390 μatm); O, other; pCO_2, partial pressure of gaseous carbon dioxide; RT, retention time; S, saccharide; SA, sugar acid; SAlc, sugar alcohol; ST, sterol; TP, terpene; U, unknown.

Table S3. Log_2 converted fold-changes in relation to pre-experimental conditions (day 0) of increased (red) and decreased (blue) detected metabolites for pCO_2 and dFe treatments in the mesocosms. A caret indicates a structure confirmed by standard or a natural sample. Metabolites tagged with '?' possessed a reverse match of 700–800 and those with '??' one of 600–700. Data represent log_2 converted fold-change of mean of triplicate mesocosms (n = 3) except for LC-DFB (n = 2) and a few data points, where we had to exclude a replicate as outlier, where n = 2 (see text). Metabolomic data have been normalized by peak sum. The column treatment refers to the treatment(s) a metabolite significantly correlated with. Abbreviations as in Table S2.